Deciphering the influence of evolutionary legacy and functional constraints on the patella: a case study in modern rhinoceroses amongst perissodactyls (#96991)

First revision

Guidance from your Editor

Please submit by **29 Jul 2024** for the benefit of the authors .

Structure and Criteria
Please read the 'Structure and Criteria' page for guidance.

Raw data check
Review the raw data.

Image check
Check that figures and images have not been inappropriately manipulated.

If this article is published your review will be made public. You can choose whether to sign your review. If uploading a PDF please remove any identifiable information (if you want to remain anonymous).

Files
Download and review all files from the materials page.

1 Tracked changes manuscript(s)
1 Rebuttal letter(s)
15 Figure file(s)
5 Table file(s)
1 Raw data file(s)

Structure and Criteria

Structure your review

The review form is divided into 5 sections. Please consider these when composing your review:

1. **BASIC REPORTING**
2. **EXPERIMENTAL DESIGN**
3. **VALIDITY OF THE FINDINGS**
4. General comments
5. Confidential notes to the editor

You can also annotate this PDF and upload it as part of your review

When ready submit online.

Editorial Criteria

Use these criteria points to structure your review. The full detailed editorial criteria is on your guidance page.

BASIC REPORTING

- Clear, unambiguous, professional English language used throughout.
- Intro & background to show context. Literature well referenced & relevant.
- Structure conforms to PeerJ standards, discipline norm, or improved for clarity.
- Figures are relevant, high quality, well labelled & described.
- Raw data supplied (see PeerJ policy).

EXPERIMENTAL DESIGN

- Original primary research within Scope of the journal.
- Research question well defined, relevant & meaningful. It is stated how the research fills an identified knowledge gap.
- Rigorous investigation performed to a high technical & ethical standard.
- Methods described with sufficient detail & information to replicate.

VALIDITY OF THE FINDINGS

- **Impact and novelty is not assessed.** Meaningful replication encouraged where rationale & benefit to literature is clearly stated.
- All underlying data have been provided; they are robust, statistically sound, & controlled.
- Conclusions are well stated, linked to original research question & limited to supporting results.

Standout reviewing tips

The best reviewers use these techniques

Tip	*Example*
Support criticisms with evidence from the text or from other sources	*Smith et al (J of Methodology, 2005, V3, pp 123) have shown that the analysis you use in Lines 241-250 is not the most appropriate for this situation. Please explain why you used this method.*
Give specific suggestions on how to improve the manuscript	*Your introduction needs more detail. I suggest that you improve the description at lines 57- 86 to provide more justification for your study (specifically, you should expand upon the knowledge gap being filled).*
Comment on language and grammar issues	*The English language should be improved to ensure that an international audience can clearly understand your text. Some examples where the language could be improved include lines 23, 77, 121, 128 – the current phrasing makes comprehension difficult. I suggest you have a colleague who is proficient in English and familiar with the subject matter review your manuscript, or contact a professional editing service.*
Organize by importance of the issues, and number your points	*1. Your most important issue* *2. The next most important item* *3. …* *4. The least important points*
Please provide constructive criticism, and avoid personal opinions	*I thank you for providing the raw data, however your supplemental files need more descriptive metadata identifiers to be useful to future readers. Although your results are compelling, the data analysis should be improved in the following ways: AA, BB, CC*
Comment on strengths (as well as weaknesses) of the manuscript	*I commend the authors for their extensive data set, compiled over many years of detailed fieldwork. In addition, the manuscript is clearly written in professional, unambiguous language. If there is a weakness, it is in the statistical analysis (as I have noted above) which should be improved upon before Acceptance.*

Deciphering the influence of evolutionary legacy and functional constraints on the patella: a case study in modern rhinoceroses amongst perissodactyls

Christophe Mallet [Corresp., 1, 2], **Alexandra Houssaye** [3]

[1] Faculty of Engineering, University of Mons, Department of Geology and Applied Geology, Mons, Belgium

[2] Institute of Natural Sciences, Operational Directorate Earth and History of Life, Brussels, Belgium

[3] Muséum National d'Histoire Naturelle, Mécanismes adaptatifs et évolution (MECADEV), UMR 7179, MNHN, CNRS, Paris, France

Corresponding Author: Christophe Mallet
Email address: christophe.mallet@edu.mnhn.fr

In mammals, the patella is the biggest sesamoid bone of the skeleton and is of crucial importance in posture and locomotion, ensuring the role of a pulley for leg extensors while protecting and stabilizing the knee joint. Despite its central biomechanical role, the relation between the shape of the patella and functional factors, such as body mass or locomotor habit, in the light of evolutionary legacy are poorly known. Here, we propose a morphofunctional investigation of the shape variation of the patella among modern rhinoceroses and more generally among perissodactyls, this order of ungulates displaying a broad range of body plan, body mass and locomotor habits, to understand how the shape of this sesamoid bone varies between species and relatively to these functional factors. Our investigation, relying on three dimensional geometric morphometrics and comparative analyses, reveals that, within Rhinocerotidae and between the three perissodactyl families, the shape of the patella strongly follows the phylogenetic affinities rather than variations in body mass. The patellar shape is more conservative than initially expected both within and between rhinoceroses, equids and tapirs. The development of a medial angle, engendering a strong mediolateral asymmetry of the patella, appears convergent in rhinoceroses and equids, while tapirs retain a symmetric bone close to the plesiomorphic condition of the order. This asymmetric patella is likely associated with the presence of a “knee locking” mechanism in both equids and rhinos. The emergence of this condition may be related to a shared locomotor habit (transverse gallop) in both groups. Our investigation underlines unexcepted evolutionary constraints on the shape of a sesamoid bone usually considered as mostly driven by functional factors.

Deciphering the influence of evolutionary legacy and functional constraints on the patella: a case study in modern rhinoceroses amongst perissodactyls

Christophe Mallet[1,2], Alexandra Houssaye[3]

[1] Operational Directorate Earth and History of Life, Institute of Natural Sciences, Brussels, Belgium

[2] Department of Geology and Applied Geology, Faculty of Engineering, University of Mons, Mons, Belgium

[3] Mécanismes adaptatifs et évolution (MECADEV), UMR 7179, MNHN, CNRS, Paris, France

Corresponding author:

Christophe Mallet

Institute of Natural Sciences, Operational Directorate Earth and History of Life

Rue Vautier, 29

1000, Brussels

Belgium

Email address: cmallet@naturalsciences.be

Abstract

In mammals, the patella is the biggest sesamoid bone of the skeleton and is of crucial importance in posture and locomotion, ensuring the role of a pulley for leg extensors while protecting and stabilizing the knee joint. Despite its central biomechanical role, the relation between the shape of the patella and functional factors, such as body mass or locomotor habit, in the light of evolutionary legacy are poorly known. Here, we propose a morphofunctional investigation of the shape variation of the patella among modern rhinoceroses and more generally among perissodactyls, this order of ungulates displaying a broad range of body plan, body mass and locomotor habits, to understand how the shape of this sesamoid bone varies between species and relatively to these functional factors. Our investigation, relying on three dimensional geometric morphometrics and comparative analyses, reveals that, within Rhinocerotidae and between the three perissodactyl families, the shape of the patella strongly follows the phylogenetic affinities rather than variations in body mass. The patellar shape is more conservative than initially expected both within and between rhinoceroses, equids and tapirs. The development of a medial angle, engendering a strong mediolateral asymmetry of the patella, appears convergent in rhinoceroses and equids, while tapirs retain a symmetric bone close to the plesiomorphic condition of the order. This asymmetric patella is likely associated with the presence of a “knee locking” mechanism in both equids and rhinos. The emergence of this condition may be related to a shared locomotor habit (transverse gallop) in both groups. Our investigation underlines unexcepted evolutionary constraints on the shape of a sesamoid bone usually considered as mostly driven by functional factors.

Introduction

In vertebrates, the shape of the skeleton is strongly influenced by structural, functional, developmental constraints, and evolutionary legacy (Seilacher, 1970, 1991; Gould, 2002). Limb bones, which function in like body support and locomotion in quadrupeds, are particularly influenced by functional constraints (Hildebrand, 1974; Hall, 2007). Variations of body plan, body mass or locomotor habits induce changes in the shape of limb elements (Hildebrand, 1974; Polly, 2007; Biewener & Patek, 2018), as observed in many clades of tetrapods (see for example Fabre et al., 2013; MacLaren & Nauwelaerts, 2016; Etienne et al., 2020a; Serio, Raia & Meloro, 2020). However, despite this intense exploration of form-function relationships focused mainly on limb long bones, smaller elements like sesamoid bones remain poorly studied. Sesamoids are small concentrations of bone generally embedded in dense connective tissue such as tendons or ligaments. They are assumed to increase leverage for muscles and tendons attached to them, while protecting the joints with which they are associated (Vickaryous & Olson, 2008). The emergence of sesamoids in some joints is directly linked to variations in mechanical loads, making them likely to carry a strong functional signal (Vickaryous & Olson, 2008; Eyal et al., 2019).

The patella is the largest sesamoid bone of the skeleton (Samuels, Regnault & Hutchinson, 2017). Long considered to form within the distal quadriceps tendon, recent findings show that the patella arises as a bony process at the anterodistal surface of the femur (Eyal et al., 2015, 2019). The patella is later embedded into the quadriceps tendon and articulates with the femur by sliding onto the distal trochlear groove. Onto the patella attach the different ends of the *musculus quadriceps* as well as the *m. gluteobiceps*, all being knee extensors (Barone, 2010a; Samuels, Regnault & Hutchinson, 2017; Etienne, Houssaye & Hutchinson, 2021) (Figure 1). The patella is also connected to the tibia through the patellar tendon, and additional lateral and medial tendons (Barone, 2010a; Samuels, Regnault & Hutchinson, 2017). The main functional role of the patella is to modify the lever arm of the *m. quadriceps*. By moving the quadriceps tendon away from the centre of rotation of the knee joint, the patella acts as a pulley and reduces the muscular energy required to extend the leg, while increasing the velocity of the rotation (Aglietti & Menchetti, 1995; Allen et al., 2017). In mammals, the patella also centralizes the forces coming from the four heads of the *m. quadriceps* into a single point of application and transmits them without friction to the tibial tuberosity. In addition, the patella acts as a protective element for the knee joint (Aglietti & Menchetti, 1995).

The functional importance of the patella led to various works that explored the biomechanical involvement of this sesamoid bone in the hindlimb movements and its mechanical advantage, mostly in humans and related hominoids (Bizarro, 1921; Ellis et al., 1980; Aglietti & Menchetti, 1995; Lovejoy, 2007; Dan et al., 2018; Pina et al., 2020; Schneider, Rooks & Besier, 2022). These aspects have been rarely addressed in other groups of amniotes (Alexander & Dimery, 1985; Chadwick et al., 2014; Allen et al., 2017), most of the studies focusing more on the evolutionary relevance of the presence or absence of the patella (Jerez, Mangione & Abdala, 2010; Ponssa, Goldberg & Abdala, 2010; Corina Vera, Laura Ponssa & Abdala, 2015; Abdala, Vera & Ponssa, 2017; Samuels, Regnault & Hutchinson, 2017). While the inner bony structure of the patella has sometimes been explored in regards to functional constraints (Raux et al., 1975; Toumi et al., 2006; Houssaye, Perthuis & Houée, 2021), the variation of its external shape, considered as relatively conservative in amniotes (Samuels, Regnault & Hutchinson, 2017), remains largely understudied. Only a few studies tried to investigate the form-function relationships at a larger interspecific scale, mostly in mammals (Valois, 1917; Raymond & Prothero, 2012; Pina et al.,

2020; Garnoeva, 2022). Therefore, the variation of the shape of the patella in relation with functional constraints remains virtually unknown in amniotes.

In this context, we chose to explore the shape variation of the patella in modern rhinoceroses and compare it with shape variation within perissodactyls (adding equids and tapirs) to investigate its relations with functional factors within a phylogenetically informed framework. Modern rhinoceroses constitute the second heaviest land mammal group after elephants (Alexander & Pond, 1992), and contrary to them, show great variations (factor of 6) of body mass (BM) among the five living species: from 600 kg for *Dicerorhinus sumatrensis* (Fischer, 1814) up to 3,500 kg for *Ceratotherium simum* (Burchell, 1817). These three-toed animals inhabit various environments from open savannas to dense rainforests, associated with diverse feeding strategies, from specialized grazers to generalist browsers (Dinerstein, 2011). They perform transverse gallop (Economou et al., 2020) and are able to reach speeds from 27 $km.h^{-1}$ for *Ceratotherium simum* to 45 $km.h^{-1}$ for *Diceros bicornis* (Garland, 1983; Alexander & Pond, 1992; Blanco, Gambini & Fariña, 2003). Body mass in rhinos can vary strongly between males and females in some species (Zschokke & Baur, 2002; Dinerstein, 2011), as well as their body plan, from long-legged black rhino *Diceros bicornis* to short-legged white rhino *C. simum*. This diversity of body construction and ecological preferences makes them a particularly well-suited group for studying the link between patellar shape and functional factors.

To expand the scope of our investigation, we chose to include in a second time other modern perissodactyls as comparative groups. The other modern perissodactyls comprise seven species of equids and four of tapirs. These two clades show less intragroup variations of size and body plan. Tapirs are forest-dwellers with a limited range of body mass (factor of 2): from 175 to 400 kg (Medici, 2011). Tapirs retain some plesiomorphic characters of the order Perissodactyla in their limbs, such as a tetradactyl manus and a tridactyl pes (MacLaren & Nauwelaerts, 2016, 2017). Their running pace is different from that of rhinos, as they perform a rotary gallop (Economou et al., 2020). As for equids, they show marked weigh variations related to domestication, although not comparable to what is observed among rhinos. If most wild equids weigh around 300 kg, some domestic horses and donkeys (such as draft races) can exceed 800 kg (factor of 2.6). In addition, equids show a highly derived limb structure adapted for running and living in open habitats, with monodactyl manus and pes (Rubenstein, 2011), associated with a transverse gallop as for rhinos (Economou et al., 2020). These three families (Rhinocerotidae, Tapiridae, Equidae) also show a gradient of stature and proportions in their limb construction, from cursorial equids to “mediportal” tapirs and “graviportal” rhinos, likely to be associated with differences in patellar shape (Eisenmann & Guérin, 1984). Recent advances in functional morphology underlined how body mass could drive – or not – the shape of limb bones in perissodactyls (MacLaren & Nauwelaerts, 2016, 2017; Hanot et al., 2017, 2018; MacLaren et al., 2018; Mallet et al., 2019, 2020, 2021, 2022; Etienne et al., 2020b), but without consideration for the patella.

Moreover, rhinoceroses and equids are known to possess a “knee locking” mechanism in their hindlimb: they are able to lock the patella and the medial patellar tendon above the medial trochlear ridge of the distal femur (Hermanson & MacFadden, 1996; Schuurman, Kersten & Weijs, 2003). Doing so, the natural flexion of the limb that could be engendered in relation with body weight becomes impossible, allowing these animals to save muscular energy for long periods of standing. Long considered as passive, *in vivo* experiments demonstrated that this mechanism does require muscular energy, even though far much less than would be needed without this apparatus (Schuurman, Kersten & Weijs, 2003). Broadly studied in domestic equids for veterinary purposes, this locking mechanism is less documented *in vivo* in rhinos and

only inferred through the shape of the distal femur but not directly through that of the patella (Shockey et al., 2008; Danaher, Shockey & Mihlbachler, 2009; Janis et al., 2012; Mihlbachler et al., 2014). A recent investigation on the microanatomy of the patella in modern perissodactyls highlighted microanatomical changes related to different functional factors, notably the presence of the knee locking mechanism (Houssaye, Perthuis & Houée, 2021). But a similar comparative investigation remains to be conducted for deciphering how functional factors are related to the external shape of the patella in this group.

For all these reasons, we chose to explore both intra- and interspecific variation of the shape of the patella among modern rhinoceroses, and to compare it with tapirs' and equids', to shed light on how this crucial sesamoid bone is influenced by functional constraints (body mass, locomotor habit, presence or not of a "knee locking" mechanism) and evolutionary legacy among Perissodactyla We relied on a 3D geometric morphometrics approach to investigate the form-function relationships on the patella. Given previous results on the shape variation of hindlimb long bones (Mallet et al., 2019, 2020) and on the inner structure of the patella (Houssaye, Perthuis & Houée, 2021) in modern rhinos, we hypothesize: (1) higher interspecific than intraspecific variation of the shape of the patella in rhinos; (2) a patellar morphology not explained by phylogenetic relations alone but also by functional factors such as body mass, presence or absence of a knee locking mechanism, and type of gallop in perissodactyls (Schuurman, Kersten & Weijs, 2003; Shockey et al., 2008; Economou et al., 2020). The consideration of equids and tapirs will allow us to situate the variation observed among rhinoceroses within the perissodactyls as a whole, and see whether the trends observed, and the hypotheses of functional links highlighted in rhinoceroses are confirmed by this contextualization on the scale of the whole family, or whether different trends between families could call into question the suggested links between form and function.

Material and Methods

Studied sample

We selected a sample composed of 54 patellae of modern perissodactyls housed in eight institutions (American Museum of Natural History, New York, USA; Powell Cotton Museum, Birchington-on-Sea, UK; Idaho Museum of Natural History, Pocatello, USA; Muséum National d'Histoire Naturelle, Paris, France; Museum of Vertebrate Zoology, Berkeley, USA; Natural History Museum, London, UK; NMB: Naturhistorisches Museum Basel, Basel, Switzerland; Institute of Natural Sciences, Brussels, Belgium) and representing the five modern species of rhinos (27 patellae), together with four modern species of tapirs (12 patellae) and 7 species (9 subspecies) of modern equids (15 patellae) (Table 1, Figure 2). We used binomial names as provided in the Handbook of Mammals of the World (vol. 2) (Dinerstein, 2011; Medici, 2011; Rubenstein, 2011). The sample includes 29 males, 17 females and 19 specimens without sex attribution. It involves only adult specimens (e.g., having fully fused epiphysis on the long bones associated with the patella), except for one specimen of unclear age but showing a general adult aspect and size and one *Equus zebra hartmannae* considered as subadult (e.g., having not fully fused epiphysis on the associated long bones) (see Table 1 for details). This last one has been kept in the sample as it was the only available specimen we encountered for this subspecies. Because of the higher intrafamilial diversity of rhinos, we chose to focus first on this group. We performed our analyses successively on rhinoceroses only, then on rhinos, equids, and tapirs together. Exploration of shape variation among equids and tapirs respectively are provided as Supplementary Data. All anatomical terms follow classic anatomical and veterinary works (Federative Committee on Anatomical Terminology, 1998; Barone, 2010b), and are given in Figure 3.

3D models

Twenty-four patellae were digitized using a structured-light three dimensional scanner (Artec Eva) and reconstructed with Artec Studio professional (v12.1.1.12 – Artec 3D, 2018). Twelve specimens were scanned using a Creaform HandySCAN 300 laser surface scanner and reconstructed using the VX Models software (Creaform, USA). Fifteen patellae were scanned using high-resolution computed tomography at the micro-CT laboratory of the Natural History Museum, London, UK (Nikon HMX 225 ST system), and six at the AST-RX platform at the Muséum National d'Histoire Naturelle, Paris (UMS 2700; GE phoenix|X-ray v|tome|xs 240), with reconstructions performed using the CT-agent software (Nikon Metrology, Leuven, Belgium), and DATOX/RES software (phoenix datos|x). Bone surfaces were extracted as meshes using Avizo 9.4 (Thermo Fisher Scientific, 2018). Three specimens were retrieved on the online deposit MorphoSource (see Table 1 for details). Only right bones were selected for digitization; when unavailable, we selected left bones instead and mirrored the 3D models before analysis using MeshLab (v2022.02 – Cignoni *et al.,* 2008). ARK identifiers of each 3D model are provided in Supplementary Table T1.

3D geometric morphometrics

We analysed the shape variation of our sample using a 3D geometric morphometrics approach. This widely used methodology allows to quantify and visualize the morphological differences between objects by comparing the spatial coordinates of landmarks placed on them (Adams, Rohlf & Slice, 2004; Zelditch et al., 2012; Mitteroecker & Schaefer, 2022). The shape of the patella was quantified by placing a set of anatomical landmarks and curve and surface sliding semi-landmarks on the meshes, as described by

Gunz, Mitteroecker, & Bookstein (2005) and Botton-Divet et al. (2016). Anatomical landmarks and curves were placed on meshes using the IDAV Landmark software (v3.0 – Wiley et al., 2005). We defined six anatomical landmarks associated with two curves allowing to cover the shape diversity of the patella in modern perissodactyls (Figure 3). We evaluated the relevance of these anatomical landmarks to describe the shape by conducting repeatability tests. We considered three specimens of *Ds. sumatrensis* chosen to display the closest morphology. We successively digitized ten times the anatomical landmarks on the three specimens to obtain thirty replications of the landmark datasets. We superimposed these landmark configurations using a Generalized Procrustes Analysis (GPA, see below) then performed a Principal Component Analysis (PCA) to visualise the placement of each repeated set of measurement relatively to each other. It appeared clearly that the variation within specimens was lower than between specimens, confirming the relevance of our landmarks to precisely describe the shape variation (see Supplementary Figure S1).

Anatomical landmarks and curve sliding semi-landmarks were placed on each specimen. A template was created for the placement of the surface sliding semi-landmark on each patella. A specimen (*C. simum* AMNH M-51854) was selected as the initial specimen on which all anatomical landmarks, curve and surface sliding semi-landmarks were placed. This specimen was selected for its average shape and size allowing to ensure the correct placement of the landmarks on all the other specimens despite the great variation of size and shape in the sample. It was then used as a template for the projection of surface sliding semi-landmarks on the surface of all other specimens. Projection was followed by a relaxation step ensuring that projected points matched the surface of the meshes. Curve and surface semi-landmarks were then slid by minimizing the bending energy of a thin plate spline (TPS) between each specimen and the template at first, then four times between the result of the previous step and the Procrustes consensus of the complete dataset (see Gunz, Mitteroecker & Bookstein, 2005; Botton-Divet et al., 2016 for details regarding this process). Once this process was complete, all landmarks could be treated as geometrically homologous. We then performed a Generalized Procrustes Analysis (GPA) to remove the effect of relative size, location and orientation of the different landmark conformations (Gower, 1975; Rohlf & Slice, 1990). Projection, relaxation, sliding processes and GPA were conducted using the “Morpho” package (v2.10 – Schlager, 2017) in the R environment (v4.2.1 – R Core Team, 2014). Details of the function parameters used are provided in the R code available as Supplementary Data.

Superimposed conformations of landmarks were then used to compute a PCA in order to reduce dimensionality (Gunz & Mitteroecker, 2013) (function “procSym” in the “Morpho” package). PC scores where then used to compute Neighbour-Joining (NJ) trees and morphospaces allowing to visualise the distribution of each individual relatively to each other. To visualise how shape varies in association with the specimen distribution, we computed theoretical shapes associated with both minimal and maximal values for the two first PCs using a TPS deformation of a template mesh. To emphasize the location of the main shape changes on the patella among the sample, we displayed the vectors of displacement between all landmarks of the two theoretical shapes using the “rgl” package (v0.109.6 – Adler & Murdoch, 2020). As described by Botton-Divet (2017) and Pintore *et al.* (2021), we applied a gradient of colour to these segments according to their distance to highlight which parts varied the most, these segments being displayed directly onto the superimposed theoretical shapes (see the R code available as Supplementary Data for details of the process).

We explored the relation between shape and specific attribution, sex and size (see below). Permutational analyses of variance (PERMANOVAs) (Costa-Pereira et al., 2016; Anderson, 2017) were performed on

PC scores against the specific attribution and sex class to test for the impact of these parameters on the patellar shape. We used the function "adonis2" in the "vegan" package (v.2.6-4) to perform PERMANOVAs (using the Euclidian method and removing lacking sex attribution with the argument "na.exclude") (Dixon, 2003). We explored allometric variation (i.e., shape variation linked to size; Hallgrímsson et al. 2009; Zelditch et al. 2012; Mitteroecker et al. 2013; Klingenberg 2016) within our sample using different approaches. Pearson's correlation tests were performed to test for correlation between the scores of the two first PCs and the centroid size of the specimens. We performed a Procrustes ANOVA (a linear regression model using Procrustes distances between species instead of covariance matrices – Goodall 1991; Adams & Otárola-Castillo 2013) with 1,000 permutations and a sequential sum of squares to quantify the shape variation related to the centroid size to highlight the of centroid size on the global shape variation. Procrustes ANOVA has been performed using the function "procD.lm" in the "geomorph" package. This set of analyses (PERMANOVA, Pearson's correlation tests, Procrustes ANOVAs) was applied respectively on rhinoceroses alone and on all perissodactyls. Detailed NJ trees and PCA plots for equids and tapirs only are provided as Supplementary Data.

Proxies of body mass

In the absence of most of the mass values of the specimens constituting our sample, we chose two proxies of body mass: 1) the centroid size (CS) of each patella, generally used to address allometric variation, defined as the square root of the sum of the square of the distance of each point to the centroid of the landmark set (Zelditch et al., 2012); it is generally considered as a good proxy of the body mass of the animal ; and 2) the minimal femoral circumference (FC) of each specimen, a measurement classically used in equations of body mass estimation. Indeed, the femur being a crucial bone for weight support in quadrupeds, its circumference is known to strongly covary with body mass (Anderson, Hall-Martin & Russell, 1985; Scott, 1990; Damuth & MacFadden, 1990; Campione & Evans, 2012; Campione, 2017). FC therefore provides a proxy of mass relatively independent of the patella itself. We used a Pearson's correlation test to evaluate the correlation between CS and FC. We also performed Procrustes ANOVAs as described above using FC instead of CS to quantify their respective relations with shape variation, both on rhinos alone and on all perissodactyls.

Phylogenetic framework

To test the presence of a phylogenetic signal in our shape data, we constructed a composite cladogram using trees previously computed on molecular data and craniodental and postcranial characters (Figure 2). Branch relations, lengths and occurrence dates were retrieved and merged following phylogenetic reconstructions proposed in recent works (Steiner & Ryder, 2011; MacLaren et al., 2018; Bai et al., 2020; Cirilli et al., 2021; Antoine et al., 2021; Liu et al., 2021; Pandolfi et al., 2021). The phylogenetic relation of *Ds. sumatrensis* relatively to the other modern species has long been debated (see Mallet et al., 2019). As recent works based on molecular and morphological data agreed on the phylogenetic position of this species (Antoine et al., 2021; Liu et al., 2021; Pandolfi et al., 2021), we considered here *Ds. sumatrensis* as sister taxon of the *Rhinoceros* genus.

We addressed the effect of phylogenetic signal on shape and centroid size in our dataset. Given the small numbers of rhino species (five), tests for phylogenetic signal were only performed on ~~the subsample containing~~ all perissodactyl species. For species represented by several specimens, we computed species mean shapes (Botton-Divet et al., 2017; Serio, Raia & Meloro, 2020; Mallet et al., 2021, 2022). We

computed a first GPA with all specimens of the second subsample (all perissodactyls) as described previously, then we computed the Procrustes consensus (or mean shape) of each species in this geometric space. These Procrustes consensuses were superimposed in a second GPA before computing a new PCA. We then addressed the effect of phylogeny on mean centroid sizes per species with the univariate K statistic (Blomberg et al., 2003), using the function "phylosig" in the "phytools" package (Revell, 2012). We also addressed the effect of phylogenetic relationships on shape data using the multivariate K statistic (K_{mult}) on PC scores (Adams, 2014). K_{mult} index allows the comparison between the rate of observed morphological change and that expected under a Brownian motion on a given phylogeny (Blomberg et al., 2003; Adams, 2014). K_{mult} was computed using the function "physignal" in the "geomorph" package (v4.0.4 – Adams & Otárola-Castillo, 2013).

According to recent works calling for a continuous approach of the p value (Wasserstein, Schirm & Lazar, 2019; Ho et al., 2019), statistic tests were considered as significant for p values ≤ 0.05 but we chose to mention and comment results having a p value between 0.05 and 0.10 as well.

Results

Shape variation within rhinoceroses

The distribution of the specimens both in the NJ tree and in the morphospace shows a clear distinction between African and Asiatic rhinos. Along the NJ tree (Figure 4), specimens of *C. simum* and *Dc. bicornis* plot together and oppose to *Ds. sumatrensis*, *R. sondaicus* and *R. unicornis*. The *Dc. bicornis* and *C. simum* specimens are mixed, as are the *R. sondaicus* and *R. unicornis* specimens. Those of *Ds. sumatrensis* form an isolated and more homogeneous cluster. The morphospace of the first two axes of the PCA, representing 47.5%, displays a similar structure (Figure 5A). PC1, which carries 33.6% of the global variance, separates African rhinos towards negative values from Asiatic rhinos towards positive values. *C. simum*, occupies the highest negative values of the axis while *R. unicornis* and *R. sondaicus* occupy the highest positive values. *Ds. sumatrensis* specimens partially overlap *R. unicornis* along the PC1. PC2 represents 13.9% of the variance and is structured by the isolation of *Ds. sumatrensis* towards the highest positive values, while all other species overlap around lower values.

A Pearson's correlation test indicates that PC1 ($r = -0.41$; $p = 0.03$) and PC2 ($r = -0.55$; $p < 0.01$) are correlated with the centroid size (Table 2). The PERMANOVA of PC scores against the specific attribution and sex of the specimen confirms a highly significant correlation between the shape of the patella and the specific attribution ($R^2 = 0.59$; $p < 0.01$), but no correlation with the sex attribution ($p = 0.47$) (Table 3).

Shape variation along PC1 is mainly related to the proximodistal extension of the base and the aspect of the medial angle (Figure 5B-a). Towards minimal values, patella display a rounded and smooth general aspect. The articular surface for the femur is concave and has a convex cranial surface. The proximal end of the medial articular surface slightly exceeds that of the lateral articular surface. The medial ridge is sigmoid in medial view, with a rounded distal part. The base is mediolaterally broad and extends slightly proximally, being only little higher than the proximal border of the articular surface. The medial angle is rounded and smooth, pointing mediodistally. Towards maximal values, the patella has a more angular general aspect. The cranial surface of the patella forms a straight dorsoventral line, before displaying a caudoventral inflexion towards the apex. The proximal end of the medial articular surface exceeds greatly that of the lateral articular surface. The medial ridge is straight in medial view, forming an almost flat relief caudally to the apex. The base forms a saliant triangle with a narrow base, and a right angle markedly higher than the proximal border of the articular surface. The medial angle forms a rounded protrusion pointing strictly medially.

Shape variation along PC2 is mainly dominated by changes in the antero-posterior broadness of the patella, the proximodistal extension of the base and the apex, and the aspect of the medial angle (Figure 5B-b). Towards minimal values, the patella has a robust general aspect, especially antero-posteriorly, with a base extending strongly proximally. The articular surface for the femur has a medial part pointing in proximal direction. In medial view, the anterior surface of the patella follows a straight line from the base before forming a marked obtuse angle towards the apex. The proximal end of the medial articular surface exceeds markedly that of the lateral articular surface. The medial ridge is slightly concave, almost straight, in medial view. The base is thick, broadly triangular and forms a saliant proximal protrusion. The medial angle forms a broad triangle pointing directly medially. The apex is thick and short. Towards maximal values, the patella is flatter antero-posteriorly, with a prominent protrusion of the apex. The

articular surface for the femur has an irregular triangular shape pointing distally. The anterior surface of the patella forms a convex surface from the base to the apex. The proximal end of the medial articular surface slightly exceeds that of the lateral articular surface. The medial ridge is concave in medial view and forms a convex relief above the apex. The base is very short and slightly extended proximally. The medial angle forms a large, rounded protrusion pointing medially. The apex expands largely and forms a saliant relief directed posterodistally.

The regression plot of the Procrustes ANOVA performed on shape against log centroid size shows a marked difference between Asiatic and African rhinos (Figure 6A). Towards maximal CS values, *C. simum* and *Dc. bicornis* plot above the line while most *R. unicornis* plot below the line. Towards minimal CS values, most *Ds. sumatrensis* plot below the line or close to it, except for one individual showing a lower centroid size compared to other specimens. Positions of *R. sondaicus* relatively to the line are hard to interpret, given the small number of individuals and the isolation of an unusually small specimen towards minimal CS values. Shape variation associated with centroid size mainly involves changes in the general proportions of the patella, as well as the relative development of the base, the medial angle and, at a lesser extent, the apex (Figure 6A and 6B). Towards high values of centroid size, the patella broadens antero-posteriorly, showing a more rounded and smooth general aspect. The base is broad and thick, slightly developed proximally, forming a convex relief posteriorly to the articular surface. The medial angle forms a smooth triangle pointing medially, distally, and posteriorly. The apex appears short and broad.

Moreover, the shape is significantly correlated with centroid size ($p < 0.01$) but accounts for only 12% of the global variance ($R^2 = 0.12$) (Table 4) The regression plot highlights a signal strongly driven by *Ds. sumatrensis* and one specimen of *R. unicornis*. When removing these two species from the Procrustes ANOVA, the correlation between shape data and size is not significant anymore ($p = 0.18$). However, the small number of individuals for these species prevents us to go further on this question. In accordance with the strong correlation between centroid size and femoral circumference (Pearson's correlation test; $r = 0.75$, $p < 0.01$), very similar results are obtained when considering the log of the minimal femoral circumference instead of the centroid size in the Procrustes ANOVA (Table 4). The regression plot of shape data against FC led to an almost similar distribution of the specimens than that obtained with CS, African rhinos plotting above the regression line while the two *Rhinoceros* species plot below and *Ds. sumatrensis* isolates towards minimal FC values (see Supplementary Figure S2A). Shape variation associated with FC are very similar to that observed with CS too, with an even more marked modification of the medial ridge of the patella (see Supplementary Figure S2B).

Shape variation between all perissodactyls

When considering the second subsample (all rhinos, tapirs, and equids), shape data carries a significant but low phylogenetic signal ($K_{mult} = 0.141$, $P < 0.01$), while the mean centroid size per species does not carry a significant phylogenetic signal ($p = 0.57$). The distribution of the specimens both in the NJ tree and in the morphospace strictly separates rhinos, equids, and tapirs (Figure 7). Among rhinos, the repartition previously observed is conserved, with clustering African and Asiatic rhinos, and one *Dc. bicornis* clustering close to *C. simum*. The species clustering is far less clear among tapirs, although the low number of specimens limits the scope of our observations. All specimens of *Tapirus indicus*, the largest and only Asiatic species of tapir, cluster together, while the other three species are less clustered. When considered separately, the different tapir species discriminate well on the PCA but stay unclustered

on the NJ tree (see Supplementary Figure S3). Among equids, most *E. quagga* plot together, as do most donkeys (*E. africanus asinus*, *E. hemionus*), far from *E. quagga*. Between them, *E. grevyi* plot together with horses (*E. ferus caballus* and *E. ferus przewalskii*). Two larger specimens of *E. asinus* are mixed among horses and quaggas, respectively. When considered alone, equids show a strong mixing, despite most zebras and horses grouping together, respectively (see Supplementary Figure S4).

The morphospace of the first two axes of the PCA, representing 65.8% of the global variance, is structured by a strict separation between the three perissodactyl families, with overlap between the species within each family (Figure 8A). PC1 carries 42.7% of the global variance and separates rhinos and equids in the negative part of the axis from tapirs which are positioned in the positive part. All equids group together with no clear structure, except for *E. hemionus*, plotting outside the equid cluster (an observation confirmed on the PCA plot of equids alone – see Supplementary Figure S4). Among each family, the separation between species is far less clear. Rhinos, to the exclusion of *Ds. sumatrensis* and to *C. simum*, although to a lesser extent, have PC1 scores that overlap those of Equidae. Among tapirs, *T. pinchaque* isolates slightly from other species, which can also be observed on the PCA plot of tapirs alone (Supplementary Figure S3). Along PC2, which accounts for 23% of the variance, rhinos, and tapirs in the negative part of the axis are separated from equids in the positive part.

PC1 and PC2 are both highly correlated with the centroid size (Pearson's correlation test: $r = -0.61$; $p < 0.01$ and $r = -0.48$; $p < 0.01$, respectively) (Table 2). PERMANOVA confirms an extremely high and significant correlation between the shape of the patella and the specific attribution ($R^2 = 0.86$; $p < 0.01$). Conversely, sex attribution is not significantly correlated with shape data ($p = 0.56$) (Table 3).

Shape variation along PC1 is mainly related to the degree of asymmetry of the patella, the extension of the medial angle, and the anteroposterior broadening of the base (Figure 8B-a). Both extreme shapes reflect respectively rhino and tapir morphotypes. Towards negative values, the anterior surface is relatively flat, with a straight anterior border forming a well-marked angle (around 125°) towards the apex. The articular surface for the femur is globally rounded and smooth. The medial ridge is sigmoid and slightly concave in medial view. The base is broad mediolaterally and extends slightly proximally. The medial angle is rounded and smooth and extends strongly mediodistally. The apex is broad and massive antero-posteriorly, and slightly expands distally. Towards positive values, the theoretical shape of the patella is strongly symmetric, with no medial angle. The anterior surface is strongly and curved from the base to the apex. The articular surface for the femur is globally rectangular with symmetric medial and lateral facets. The medial ridge is concave in medial view, the rounded distal part towards the apex protruding only slightly. The base is well-developed and broad antero-posteriorly, ending in a marked knob pointing medio-proximally. The medial angle is almost absent, reduced to a smooth relief along the medial border of the articular surface. The apex is thin, wedge-shaped, slightly extended distally relatively to the articular surface.

Along PC2, shape variation is mainly related to the development and aspect of the base and of the medial angle (Figure 8B-b). Towards minimal values, the shape displays a "rhino-like" general aspect with a marked mediolateral compression. The base forms a salient relief extending markedly proximally. The medial angle is rounded, smooth and extends in medial direction. Towards maximal values, patellae are shaped like a triangular-based pyramid. The anterior surface is strongly convex, extending markedly anteriorly. In medial view, the anterior border of the patella forms a 45-degrees downward slope towards the apex. The articular surface for the femur forms a marked angle pointing medially. The proximal end

of the medial articular surface is situated below that of the lateral articular surface. The medial ridge forms a smooth sigmoid in medial view, the proximal part overhanging the articular surface in posterior direction. The base expands massively in anterior direction and forms a large flat surface strongly inclined distally towards the medial angle. No marked relief is visible on the surface of the base. The medial angle is broad and rounded, extending strongly medio-distally. The apex is short antero-posteriorly. Views of patellar mean shapes for each species of the dataset are displayed in the Supplementary Figure S5.

Shape is significantly correlated with centroid size (Procrustes ANOVA: $R^2 = 0.22$; $p < 0.01$) (Table 4). The regression plot of shape against log centroid size shows a limited spreading of the specimens around the regression line (Figure 9A). Towards maximal CS values, *C. simum* and *Ds. sumatrensis* are now mostly above the regression line while *R. unicornis* plot mostly below. Once again, the position of the few specimens of *Dc. bicornis* and *R. sondaicus* remains hard to interpret. Almost all equids plot above the regression line with few exceptions: *E. caballus* and two *E. asinus*, one of which being a draught breed with the highest CS value of the sample. All tapirs plot together below the regression line and are ordered from the least body mass to the greatest one along the centroid size values. Shape variation associated with centroid size mainly reflects differences between tapirs for minimal values and rhinos for maximal values. Changes in centroid size among perissodactyls involve changes in the general asymmetry of the patella, the relative development of the medial angle and the cranio-caudal broadening of the bone (Figure 9A and 9B). As for rhinos alone, the femoral circumference among all perissodactyls is highly correlated to the centroid size of the patella ($r = 0.88$, $p < 0.01$). Consequently, shape is also correlated with femoral circumference (Procrustes ANOVA: $R^2 = 0.26$; $p < 0.01$) (Table 4), with a regression plot and associated shape variation very similar to those observed for CS (see Supplementary Figure S6).

Discussion

Intra- and interfamily variation of shape

Our results highlight a marked distinction between African and Asiatic rhino clades, despite important weight variations within these two groups, suggesting that the shape of the patella among rhinoceroses is highly related to phylogenetic affinities prior to body mass. Each rhino species possesses a unique patellar shape. This supports our first hypothesis that interspecific variation of patellar shape is stronger than intraspecific variation of patellar shape. In the hindlimb, the patella articulates directly with the trochlear groove of the femur, while it is linked with the tibia by only ligaments. Moreover, the patella in mammals is known to separate from the femur in the early developmental stages of the embryo (Eyal et al., 2015, 2019). The patella and the femur are therefore strongly bonded bones, both on functional and developmental aspects. These observations are congruent with previous results suggesting that femoral shape variation is also more greatly driven by phylogenetic affinities over body mass, especially the distal part directly linked with the patella (Mallet et al., 2019, 2022).

Although statistically limited, our results allow one to draw preliminary considerations on the relation between the shape of the patella and sex attribution among modern rhinoceroses. Our current data do not detect a clear shape distinction between males and females. The appendicular skeleton of modern rhinos is weakly dimorphic (Guérin, 1980; Mallet et al., 2019) with phenotypic dimorphic traits being generally limited to larger horns or slightly heavier males or females (depending on the species) (Dinerstein, 1991, 2011; Zschokke & Baur, 2002). As seen above, body mass variation does not strongly influence the patellar shape in rhinos. Our results suggest that the patella does not bear a significant dimorphic signal among modern rhinos.

Among perissodactyls, the three families (Tapiridae, Equidae, Rhinocerotidae) are distinct, tapirs being very different from both rhinoceroses and equids. This result does not reflect the phylogenetic relationships among the family Perissodactyla, rhinos and tapirs being sister taxa, but rather rely on the shared high development of the medial angle, creating a strong mediolateral asymmetry, absent in tapirs. The patella condition in tapirs is plesiomorphic and thus very close to the one observed in early perissodactyls, although this bone is barely described in literature (Bai et al., 2017), while rhinos and equids show a more derived condition relatively to the supposed basal shape.

Furthermore, intrafamily variations reveal to be higher among rhinos than among equids and tapirs. These relative differences in variation within the three families may be related to their respective evolutionary history. Divergences between the different rhino clades occurred from the Oligocene to Miocene (Figure 2) (Bai et al., 2020; Antoine et al., 2021; Liu et al., 2021). Tapir branches also diverged during the Miocene (Steiner & Ryder, 2011; MacLaren et al., 2018) but this clade remained monogeneric, contrary to rhinos. Equids, another monogeneric clade, includes species that diverged very recently during the Pliocene (Steiner & Ryder, 2011; Cirilli et al., 2021). The deeper ancestry of crown Rhinocerotidae, compared to that of crown Tapiridae and crown Equidae, may explain the higher diversity of patellar shape in this clade relatively to its sister groups.

Microanatomical investigations on the patella of modern perissodactyls revealed no increase in compactness with body mass and no thickening of the cortex on muscle insertions but on the patellar ligament on the cranial side of the bone (Houssaye, Perthuis & Houée, 2021). These results are consistent with ours on the rather conservative nature of this bone in relation to body mass variation. Conversely, the

microanatomy distinguishes more rhinos and equids than rhinos and tapirs, contrary to our results, underlining a decoupling between the external morphology of the patella and its internal structure among perissodactyls.

Functional constraints and "knee locking" mechanism

In modern rhinoceroses, our results underline a significant relation between the patellar shape and both its size and the femoral circumference, an excellent proxy of body mass in quadrupeds (Scott, 1990; Campione & Evans, 2012; Campione, 2017). The centroid size of the patella therefore appears directly related to body weight in rhinos, as previously observed for long bones and ankle bones in these animals (Mallet et al., 2019; Etienne et al., 2020b). However, shape relation with size is limited, allometry accounting for only 12% of the observed shape variation. The influence of body mass on the patellar shape therefore appears as secondary relatively to phylogenetic relationships in rhinos, which partially contradicts our second hypothesis, postulating a stronger effect of mass over phylogeny on the patellar shape. Thus, despite the central functional role of the patella in the knee, and the high stress linked to body mass exerted on this joint, the influence of the weight is much more limited than expected.

Variation linked to size mainly affects the base, the medial angle, and the lateral edge of the patella, as well as the cranial surface. All these areas are insertions for knee extensors, respectively the *m. rectus femoris*, the *m. vastus medialis*, the *m. vastus lateralis* (all three, together with the *m. vastus intermedius*, forming the *m. quadriceps*) and the *m. gluteobiceps* (Etienne, Houssaye & Hutchinson, 2021) (Figure 1). The flattening of the base and the general craniocaudal broadening of the patella in heavy rhino species likely provide more surface area for the insertion of stronger *m. rectus femoris* and *m. gluteobiceps*, while in lighter rhinos the proximal development of the base seems to increase the attachment surface for the *m. vastus lateralis* and *m. vastus medialis* instead. This configuration may reflect that heavy rhinos rely more on central hip muscles, such as the *m. rectus femoris,* to stabilize the knee while lighter rhinos rely on medial and caudal muscles of the *m. quadriceps*, maybe ensuring more manoeuvrability for this joint. Unfortunately, the scarcity of myological data for lighter rhino species (Etienne, Houssaye & Hutchinson, 2021) and the lack of *in vivo* observations prevent us from making further inference between the patellar shape and its relation to attached muscles.

The allometric relation is more strongly marked when considering all perissodactyls (Figure 9), allometry accounting for 23% of the observed variation. However, body mass alone seems insufficient to explain the shape variation among perissodactyls. A developed medial angle exists both in equids and rhinos but not in tapirs, even though tapirs and equids are in the same range of body mass (hundreds of kilograms), while rhinos can reach several metric tons (Table 1). Medial angle is associated with the presence of a "knee locking" mechanism (Shockey, 2001; Schuurman, Kersten & Weijs, 2003; Janis et al., 2012). Largely studied through the anatomy of the distal femora, this mechanism has barely been considered on the patellar side (Kappelman, 1988; Hermanson & MacFadden, 1996; Janis et al., 2012; Etienne et al., 2020a). Our results do confirm the high correspondence between the presence of a developed medial angle on the patella and that of a developed medial trochlear ridge on the femur (Hermanson & MacFadden, 1996; Mallet et al., 2019). This developed medial angle shared between equids and rhinos therefore appears as convergent in the two clades, although it does not seem perfectly homologous. Indeed, while the medial angle in equids is extended by a parapatellar cartilage on which the medial patellar ligament attaches (Hermanson & MacFadden, 1996, fig. 2), this cartilage seems absent in rhinoceroses (or is little developed – C. Etienne, pers. com.), where the bony angle is more extended

medially than in equids. As shown in our results, the medial angle in rhinos is more extended and ossified medially compared to equids. This could be directly related to their higher body mass, making cartilage alone insufficient to support the weight of the body and ensure an efficient "knee locking". This would be in line with our second hypothesis, assuming different shapes of patella to ensure an efficient "knee locking" mechanism between equids and rhinos.

Similarly, the craniocaudal development of the base in equids offers a larger surface area for insertions of knee extensors, these muscles being more powerful in equids than in rhinos compared to the respective size of these animals (Etienne, Houssaye & Hutchinson, 2021). Myological data lack for tapirs but the reduced surface of the base likely indicates reduced muscle insertions and, therefore, less powerful knee extensors in these animals. Such a craniocaudal development shifts the insertion of the extensor muscles away from the axis of rotation of the knee, thus increasing the moment arm of the joint and the muscular efficiency. This craniocaudal development of the patella in equids likely underlines the extreme cursorial specialization of this clade, while the condition in rhinos appears more as a trade-off between the support of their high body mass, their ability to reach a relatively high speed, and their evolutionary legacy.

The convergent emergence of the knee asymmetry in these clades remain barely understood among ungulates, various authors having supposed a link with either locomotor habit, feeding behaviour or body mass (Kappelman, 1988; Hermanson & MacFadden, 1996; Shockey, 2001; Shockey et al., 2008; Danaher, Shockey & Mihlbachler, 2009; Janis et al., 2012; Mihlbachler et al., 2014; Etienne et al., 2020a). Locomotor habit shows a marked dichotomy between these clades. Rhinos and equids both practice a transverse gallop while tapirs practice rotatory gallop, involving different limb loadings during the gallop phases (Economou et al., 2020). Rotatory gallop involves a phase where both hindlimbs hit the ground, while this never happen in transverse gallop, leading to higher mechanical stress exerted into a single limb in the latter gait. While equids present an extreme cursorial specialization associated with relatively low mass (Carrano, 1999), weight-bearing rhinos are still able to reach high speed despite weighting several tons (Alexander & Pond, 1992; Etienne, Houssaye & Hutchinson, 2021). An asymmetrical patella could be related to the emergence of a similar gallop in both equids and rhinos, compared to tapirs. Differences in body mass may then explain the further divergences existing in patellar shape between these two clades practicing transverse gallop. Further investigations including a large set of fossil perissodactyls are needed to sharpen the understanding of this puzzling feature and the functional advantages of this presence or absence in ungulates.

Conclusion

Our investigation of the shape of the patella among modern rhinoceroses and related extant perissodactyls reveals a higher interspecific than intraspecific morphological variation. Contrary to our predictions, and despite its central functional role in the knee joint and its implication in locomotion, the patella is little affected by variation of body mass between and within species. Rather, the patellar shape follows clear morphotypes existing in each species and even more marked at the scale of the family. This strong shape conservatism may be directly related to its developmental origin, shared with the femur, another bone whose shape has been proved to be highly linked to phylogenetic affinities before functional constraints in perissodactyls. Despite a strong evolutionary legacy leading to a relative shape inertia, the shared presence of a medial angle in rhinos and equids constitutes a clear case of morphological convergence highlighting that functional constraints are also at work on the shape of this sesamoid bone. This asymmetric conformation of the patella is related to a "knee locking" mechanism and maybe to the shared

emergence of transverse gallop in both clades. Within this convergence, rhinos present additional shape modifications that may be related to the support of a heavy mass. Further investigations of the shape of the patella among a larger set of extinct Perissodactyla may be helpful for better understanding the morphofunctional evolution of this sesamoid bone in mammals.

Acknowledgments

The authors warmly thank all the curators of the visited institutions for granting us access to the studied specimens: E. Hoeger and S. Ketelsen (American Museum of Natural History, New York, USA), C. West, R. Jennings, M. Cobb (Powell Cotton Museum, Birchington-on-Sea, UK), J. Lesur, A. Verguin (Muséum National d'Histoire Naturelle, Paris, France), R. Portela-Miguez (Natural History Museum, London, UK), F. Zachos, A. Bibl (Naturhistorisches Museum Wien, Vienna, Austria), O. Pauwels, S. Bruaux (Royal Belgian Institute of Natural Sciences, Brussels, Belgium), E. Gilissen (Royal Museum for Central Africa, Tervuren, Belgium) and A. H. van Heteren (Zoologische Staatssammlung München, Munich, Germany). We acknowledge the EDDyLab (ULiège, Belgium) and V. Fischer for allowing us to use the Creaform HandySCAN 300 laser surface scanner to scan several specimens. The authors also warmly thank L. Moizo (MNHN, Paris, France), who reconstructed and extracted 3D models during its MSc internship. We acknowledge C. Étienne (MNHN, Paris, France) for precious indications regarding the knee anatomy in rhinos, and J. Gônet (MNHN, Paris, France) for digitizing some additional patellas. We would like to thank J. Wölfer (Humboldt-Universität zu Berlin, Germany) and an anonymous reviewer for their precious comments that improved the quality of the manuscript.

References

Abdala V, Vera MC, Ponssa ML. 2017. On the Presence of the Patella in Frogs. *The Anatomical Record* 300:1747–1755. DOI: 10.1002/ar.23629.

Adams DC. 2014. A generalized K statistic for estimating phylogenetic signal from shape and other high-dimensional multivariate data. *Systematic Biology* 63:685–697. DOI: 10.1093/sysbio/syu030.

Adams DC, Otárola-Castillo E. 2013. geomorph: an r package for the collection and analysis of geometric morphometric shape data. *Methods in Ecology and Evolution* 4:393–399. DOI: 10.1111/2041-210X.12035.

Adams DC, Rohlf FJ, Slice DE. 2004. Geometric morphometrics: Ten years of progress following the 'revolution.' *Italian Journal of Zoology* 71:5–16. DOI: 10.1080/11250000409356545.

Adler D, Murdoch D. 2020. rgl: 3d visualization device system (OpenGL).

Aglietti P, Menchetti PPM. 1995. Biomechanics of the Patellofemoral Joint. In: Scuderi GR ed. *The Patella*. New York, NY: Springer, 25–48. DOI: 10.1007/978-1-4612-4188-1_3.

Alexander RM, Dimery NJ. 1985. The significance of sesamoids and retro-articular processes for the mechanics of joints. *Journal of Zoology* 205:357–371. DOI: https://doi.org/10.1111/j.1469-7998.1985.tb05622.x.

Alexander RM, Pond CM. 1992. Locomotion and bone strength of the white rhinoceros, Ceratotherium simum. *Journal of Zoology* 227:63–69. DOI: 10.1111/j.1469-7998.1992.tb04344.x.

Allen VR, Kambic RE, Gatesy SM, Hutchinson JR. 2017. Gearing effects of the patella (knee extensor muscle sesamoid) of the helmeted guineafowl during terrestrial locomotion. *Journal of Zoology* 303:178–187. DOI: https://doi.org/10.1111/jzo.12485.

Anderson MJ. 2017. Permutational Multivariate Analysis of Variance (PERMANOVA). In: *Wiley StatsRef: Statistics Reference Online*. John Wiley & Sons, Ltd, 1–15. DOI: 10.1002/9781118445112.stat07841.

600 Anderson JF, Hall-Martin A, Russell DA. 1985. Long-bone circumference and weight in mammals, birds
601 and dinosaurs. *Journal of Zoology* 207:53–61. DOI: 10.1111/j.1469-7998.1985.tb04915.x.
602 Antoine P-O, Reyes MC, Amano N, Bautista AP, Chang C-H, Claude J, De Vos J, Ingicco T. 2021. A new
603 rhinoceros clade from the Pleistocene of Asia sheds light on mammal dispersals to the
604 Philippines. *Zoological Journal of the Linnean Society* 194:416–430. DOI:
605 10.1093/zoolinnean/zlab009.
606 Artec 3D. 2018. Artec Studio Professional.
607 Bai B, Meng J, Wang Y-Q, Wang H-B, Holbrook L. 2017. Osteology of The Middle Eocene Ceratomorph
608 Hyrachyus modestus (Mammalia, Perissodactyla). *Bulletin of the American Museum of Natural*
609 *History*:1–70. DOI: 10.1206/0003-0090-413.1.1.
610 Bai B, Meng J, Zhang C, Gong Y-X, Wang Y-Q. 2020. The origin of Rhinocerotoidea and phylogeny of
611 Ceratomorpha (Mammalia, Perissodactyla). *Communications Biology* 3:1–16. DOI:
612 10.1038/s42003-020-01205-8.
613 Barone R. 2010a. *Anatomie comparée des mammifères domestiques. Tome 2 : Arthrologie et myologie*.
614 Paris: Vigot Frères.
615 Barone R. 2010b. *Anatomie comparée des mammifères domestiques. Tome 1 : Ostéologie*. Paris: Vigot
616 Frères.
617 Biewener AA, Patek SN. 2018. *Animal Locomotion*. New York: Oxford University Press.
618 Bizarro AH. 1921. On Sesamoid and Supernumerary Bones of the Limbs. *Journal of Anatomy* 55:256–
619 268.
620 Blanco RE, Gambini R, Fariña RA. 2003. Mechanical model for theoretical determination of maximum
621 running speed in mammals. *Journal of Theoretical Biology* 222:117–125. DOI: 10.1016/S0022-
622 5193(03)00019-5.

623 Blomberg SP, Garland T, Ives AR, Crespi B. 2003. Testing for phylogenetic signal in comparative data:
624 behavioral traits are more labile. *Evolution* 57:717–745. DOI: 10.1554/0014-
625 3820(2003)057[0717:TFPSIC]2.0.CO;2.
626 Botton-Divet L. 2017. The Form-Function relationships in the process of secondary adaptation to an
627 aquatic life. PhD Thesis Thesis. Paris: Université Sorbonne Paris Cité.
628 Botton-Divet L, Cornette R, Fabre A-C, Herrel A, Houssaye A. 2016. Morphological Analysis of Long Bones
629 in Semi-aquatic Mustelids and their Terrestrial Relatives. *Integrative and Comparative Biology*
630 56:1298–1309. DOI: 10.1093/icb/icw124.
631 Botton-Divet L, Cornette R, Houssaye A, Fabre A-C, Herrel A. 2017. Swimming and running: a study of
632 the convergence in long bone morphology among semi-aquatic mustelids (Carnivora:
633 Mustelidae). *Biological Journal of the Linnean Society* 121:38–49. DOI:
634 10.1093/biolinnean/blw027.
635 Campione NE. 2017. Extrapolating body masses in large terrestrial vertebrates. *Paleobiology* 43:693–
636 699. DOI: 10.1017/pab.2017.9.
637 Campione NE, Evans DC. 2012. A universal scaling relationship between body mass and proximal limb
638 bone dimensions in quadrupedal terrestrial tetrapods. *BMC Biology* 10:1–21. DOI:
639 10.1186/1741-7007-10-60.
640 Carrano MT. 1999. What, if anything, is a cursor? Categories versus continua for determining locomotor
641 habit in mammals and dinosaurs. *Journal of Zoology* 247:29–42. DOI: 10.1111/j.1469-
642 7998.1999.tb00190.x.
643 Chadwick KP, Regnault S, Allen V, Hutchinson JR. 2014. Three-dimensional anatomy of the ostrich
644 (Struthio camelus) knee joint. *PeerJ* 2:e706. DOI: 10.7717/peerj.706.

645 Cignoni P, Callieri M, Corsini M, Dellepiane M, Ganovelli F, Ranzuglia G. 2008. *MeshLab: an Open-Source*
646 *Mesh Processing Tool*. The Eurographics Association. DOI:
647 http://dx.doi.org/10.2312/LocalChapterEvents/ItalChap/ItalianChapConf2008/129-136.
648 Cirilli O, Pandolfi L, Rook L, Bernor RL. 2021. Evolution of Old World Equus and origin of the zebra-ass
649 clade. *Scientific Reports* 11:10156. DOI: 10.1038/s41598-021-89440-9.
650 Corina Vera M, Laura Ponssa M, Abdala V. 2015. Further Data on Sesamoid Identity from Two Anuran
651 Species. *The Anatomical Record* 298:1376–1394. DOI: 10.1002/ar.23158.
652 Costa-Pereira R, Araújo MS, Paiva F, Tavares LER. 2016. Functional morphology of the tetra fish Astyanax
653 lacustris differs between divergent habitats in the Pantanal wetlands. *Journal of Fish Biology*
654 89:1450–1458. DOI: 10.1111/jfb.13026.
655 Damuth JD, MacFadden BJ. 1990. *Body Size in Mammalian Paleobiology: Estimation and Biological*
656 *Implications*. Cambridge University Press.
657 Dan M, Parr W, Broe D, Cross M, Walsh WR. 2018. Biomechanics of the knee extensor mechanism and
658 its relationship to patella tendinopathy: A review. *Journal of Orthopaedic Research* 36:3105–
659 3112. DOI: https://doi.org/10.1002/jor.24120.
660 Danaher K, Shockey BJ, Mihlbachler MC. 2009. Perissodactyl patella: morphological variation and
661 phylogenetic signifiance in a neglected element. *Journal of Vertebrate Paleontology* 29:85A.
662 Dinerstein E. 1991. Sexual Dimorphism in the Greater One-Horned Rhinoceros (Rhinoceros unicornis).
663 *Journal of Mammalogy* 72:450–457. DOI: 10.2307/1382127.
664 Dinerstein E. 2011. Family Rhinocerotidae (Rhinoceroses). In: Wilson DE, Mittermeier RA eds. *Handbook*
665 *of the Mammals of the World*. Barcelona: Don E. Wilson & Russel A. Mittermeier, 144–181.
666 Dixon P. 2003. VEGAN, a package of R functions for community ecology. *Journal of Vegetation Science*
667 14:927–930. DOI: 10.1111/j.1654-1103.2003.tb02228.x.

668 Economou G, McGrath M, Wajsberg J, Granatosky MC. 2020. Perissodactyla Locomotion. In: Vonk J,
669 Shackelford T eds. *Encyclopedia of Animal Cognition and Behavior*. Cham: Springer International
670 Publishing, 1–8. DOI: 10.1007/978-3-319-47829-6_887-1.
671 Eisenmann V, Guérin C. 1984. Morphologie fonctionnelle et environnement chez les périssodactyles.
672 *Geobios* 17:69–74. DOI: 10.1016/S0016-6995(84)80158-8.
673 Ellis MI, Seedhom BB, Wright V, Dowson D. 1980. An Evaluation of the Ratio between the Tensions along
674 the Quadriceps Tendon and the Patellar Ligament. *Engineering in Medicine* 9:189–194. DOI:
675 10.1243/EMED_JOUR_1980_009_049_02.
676 Etienne C, Filippo A, Cornette R, Houssaye A. 2020a. Effect of mass and habitat on the shape of limb long
677 bones: A morpho-functional investigation on Bovidae (Mammalia: Cetartiodactyla). *Journal of*
678 *Anatomy* 238:886–904. DOI: https://doi.org/10.1111/joa.13359.
679 Etienne C, Houssaye A, Hutchinson JR. 2021. Limb myology and muscle architecture of the Indian
680 rhinoceros Rhinoceros unicornis and the white rhinoceros Ceratotherium simum (Mammalia:
681 Rhinocerotidae). *PeerJ* 9:e11314. DOI: 10.7717/peerj.11314.
682 Etienne C, Mallet C, Cornette R, Houssaye A. 2020b. Influence of mass on tarsus shape variation: a
683 morphometrical investigation among Rhinocerotidae (Mammalia: Perissodactyla). *Biological*
684 *Journal of the Linnean Society* 129:950–974. DOI: 10.1093/biolinnean/blaa005.
685 Eyal S, Blitz E, Shwartz Y, Akiyama H, Schweitzer R, Zelzer E. 2015. On the development of the patella.
686 *Development* 142:1831–1839. DOI: 10.1242/dev.121970.
687 Eyal S, Rubin S, Krief S, Levin L, Zelzer E. 2019. Common cellular origin and diverging developmental
688 programs for different sesamoid bones. *Development* 146:dev167452. DOI:
689 10.1242/dev.167452.

690 Fabre A-C, Cornette R, Peigné S, Goswami A. 2013. Influence of body mass on the shape of forelimb in
691 musteloid carnivorans. *Biological Journal of the Linnean Society* 110:91–103. DOI:
692 10.1111/bij.12103.
693 Federative Committee on Anatomical Terminology. 1998. *Terminologia Anatomica*. Georg Thieme
694 Verlag.
695 Garland T. 1983. The relation between maximal running speed and body mass in terrestrial mammals.
696 *Journal of Zoology* 199:157–170. DOI: 10.1111/j.1469-7998.1983.tb02087.x.
697 Garnoeva R. 2022. Patellar Morphology in Small Breed Dogs With Medial Patellar Luxation. *Egyptian*
698 *Journal of Veterinary Sciences* 53:403–408. DOI: 10.21608/ejvs.2022.121266.1327.
699 Goodall C. 1991. Procrustes Methods in the Statistical Analysis of Shape. *Journal of the Royal Statistical*
700 *Society: Series B (Methodological)* 53:285–321. DOI: 10.1111/j.2517-6161.1991.tb01825.x.
701 Gould SJ. 2002. *The Structure of Evolutionary Theory*. Cambridge, Massachusetts; London, England:
702 Harvard University Press.
703 Gower JC. 1975. Generalized procrustes analysis. *Psychometrika* 40:33–51. DOI: 10.1007/BF02291478.
704 Guérin C. 1980. Les Rhinocéros (Mammalia, Perissodactyla) du Miocène terminal au Pléistocène
705 supérieur en Europe occidentale. Comparaison avec les espèces actuelles. Documents du
706 Laboratoire de Géologie de l'Université de Lyon Thesis.
707 Gunz P, Mitteroecker P. 2013. Semilandmarks: a method for quantifying curves and surfaces. *Hystrix, the*
708 *Italian Journal of Mammalogy* 24:103–109.
709 Gunz P, Mitteroecker P, Bookstein FL. 2005. Semilandmarks in Three Dimensions. In: Slice DE ed.
710 *Modern Morphometrics in Physical Anthropology*. Developments in Primatology: Progress and
711 Prospects. Boston, MA: Slice, D. E., 73–98. DOI: 10.1007/0-387-27614-9_3.
712 Hall BK. 2007. *Fins into Limbs: Evolution, Development, and Transformation*. University of Chicago Press.

713 Hallgrímsson B, Jamniczky H, Young NM, Rolian C, Parsons TE, Boughner JC, Marcucio RS. 2009.
714 Deciphering the Palimpsest: Studying the Relationship Between Morphological Integration and
715 Phenotypic Covariation. *Evolutionary Biology* 36:355–376. DOI: 10.1007/s11692-009-9076-5.
716 Hanot P, Herrel A, Guintard C, Cornette R. 2017. Morphological integration in the appendicular skeleton
717 of two domestic taxa: the horse and donkey. *Proc. R. Soc. B* 284:20171241. DOI:
718 10.1098/rspb.2017.1241.
719 Hanot P, Herrel A, Guintard C, Cornette R. 2018. The impact of artificial selection on morphological
720 integration in the appendicular skeleton of domestic horses. *Journal of Anatomy* 232:657–673.
721 DOI: 10.1111/joa.12772.
722 Hermanson JW, MacFadden BJ. 1996. Evolutionary and functional morphology of the knee in fossil and
723 extant horses (Equidae). *Journal of Vertebrate Paleontology* 16:349–357. DOI:
724 10.1080/02724634.1996.10011321.
725 Hildebrand M. 1974. *Analysis of vertebrate structure*. New York: John Wiley & Sons.
726 Ho J, Tumkaya T, Aryal S, Choi H, Claridge-Chang A. 2019. Moving beyond P values: data analysis with
727 estimation graphics. *Nature Methods* 16:565–566. DOI: 10.1038/s41592-019-0470-3.
728 Houssaye A, Perthuis A de, Houée G. 2021. Sesamoid bones also show functional adaptation in their
729 microanatomy—The example of the patella in Perissodactyla. *Journal of Anatomy* n/a. DOI:
730 10.1111/joa.13530.
731 Janis CM, Shoshitaishvili B, Kambic R, Figueirido B. 2012. On their knees: distal femur asymmetry in
732 ungulates and its relationship to body size and locomotion. *Journal of Vertebrate Paleontology*
733 32:433–445. DOI: 10.1080/02724634.2012.635737.
734 Jerez A, Mangione S, Abdala V. 2010. Occurrence and distribution of sesamoid bones in squamates: a
735 comparative approach. *Acta Zoologica* 91:295–305. DOI: 10.1111/j.1463-6395.2009.00408.x.

736 Kappelman J. 1988. Morphology and locomotor adaptations of the bovid femur in relation to habitat.
737 *Journal of Morphology* 198:119–130. DOI: 10.1002/jmor.1051980111.
738 Klingenberg CP. 2016. Size, shape, and form: concepts of allometry in geometric morphometrics.
739 *Development Genes and Evolution* 226:113–137. DOI: 10.1007/s00427-016-0539-2.
740 Liu S, Westbury MV, Dussex N, Mitchell KJ, Sinding M-HS, Heintzman PD, Duchêne DA, Kapp JD, Seth J
741 von, Heiniger H, Sánchez-Barreiro F, Margaryan A, André-Olsen R, Cahsan BD, Meng G, Yang C,
742 Chen L, Valk T van der, Moodley Y, Rookmaaker K, Bruford MW, Ryder O, Steiner C, Sonsbeek
743 LGRB, Vartanyan S, Guo C, Cooper A, Kosintsev P, Kirillova I, Lister AM, Marques-Bonet T,
744 Gopalakrishnan S, Dunn RR, Lorenzen ED, Shapiro B, Zhang G, Antoine P-O, Dalén L, Gilbert MTP.
745 2021. Ancient and modern genomes unravel the evolutionary history of the rhinoceros family.
746 *Cell* 184:4874-4885.e16. DOI: 10.1016/j.cell.2021.07.032.
747 Lovejoy CO. 2007. The natural history of human gait and posture: Part 3. The knee. *Gait & Posture*
748 25:325–341. DOI: 10.1016/j.gaitpost.2006.05.001.
749 MacLaren JA, Hulbert Jr RC, Wallace SC, Nauwelaerts S. 2018. A morphometric analysis of the forelimb in
750 the genus Tapirus (Perissodactyla: Tapiridae) reveals influences of habitat, phylogeny and size
751 through time and across geographical space. *Zoological Journal of the Linnean Society* 20:1–17.
752 MacLaren JA, Nauwelaerts S. 2016. A three-dimensional morphometric analysis of upper forelimb
753 morphology in the enigmatic tapir (Perissodactyla: Tapirus) hints at subtle variations in
754 locomotor ecology. *Journal of Morphology* 277:1469–1485. DOI: 10.1002/jmor.20588.
755 MacLaren JA, Nauwelaerts S. 2017. Interspecific variation in the tetradactyl manus of modern tapirs
756 (Perissodactyla: Tapirus) exposed using geometric morphometrics. *Journal of Morphology*
757 278:1517–1535. DOI: 10.1002/jmor.20728.

758 Mallet C, Billet G, Cornette R, Alexandra Houssaye A. 2022. Adaptation to graviportality in
759 Rhinocerotoidea? An investigation through the long bone shape variation in their hindlimb.
760 *Zoological Journal of the Linnean Society* 196:1235–1271. DOI: 10.1093/zoolinnean/zlac007.
761 Mallet C, Billet G, Houssaye A, Cornette R. 2020. A first glimpse at the influence of body mass in the
762 morphological integration of the limb long bones: an investigation in modern rhinoceroses.
763 *Journal of Anatomy* 237:704–726. DOI: 10.1111/joa.13232.
764 Mallet C, Cornette R, Billet G, Houssaye A. 2019. Interspecific variation in the limb long bones among
765 modern rhinoceroses—extent and drivers. *PeerJ* 7:e7647. DOI: 10.7717/peerj.7647.
766 Mallet C, Houssaye A, Cornette R, Billet G. 2021. Long bone shape variation in the forelimb of
767 Rhinocerotoidea – Relation with size, body mass and body proportions. *Zoological Journal of the*
768 *Linnean Society* 196:1201–1234. DOI: 10.1093/zoolinnean/zlab095.
769 Medici EP. 2011. Family Tapiridae (Tapirs). In: Wilson DE, Mittermeier RA eds. *Handbook of the*
770 *mammals of the world*. Barcelona: Lynx Edicions, 182–203.
771 Mihlbachler MC, Lau T, Kapner D, Shockey BJ. 2014. Coevolution of the shoulder and knee in Ungulates:
772 Implications of the evolution of locomotion and standing.
773 Mitteroecker P, Gunz P, Windhager S, Schaefer K. 2013. A brief review of shape, form, and allometry in
774 geometric morphometrics, with applications to human facial morphology. *Hystrix, the Italian*
775 *Journal of Mammalogy* 24:59–66. DOI: 10.4404/hystrix-24.1-6369.
776 Mitteroecker P, Schaefer K. 2022. Thirty years of geometric morphometrics: Achievements, challenges,
777 and the ongoing quest for biological meaningfulness. *American Journal of Biological*
778 *Anthropology* 178:181–210. DOI: 10.1002/ajpa.24531.
779 Pandolfi L, Antoine P-O, Bukhsianidze M, Lordkipanidze D, Rook L. 2021. Northern Eurasian
780 rhinocerotines (Mammalia, Perissodactyla) by the Pliocene–Pleistocene transition: phylogeny

781 and historical biogeography. *Journal of Systematic Palaeontology*:1–27. DOI:
782 10.1080/14772019.2021.1995907.
783 Pina M, DeMiguel D, Puigvert F, Marcé-Nogué J, Moyà-Solà S. 2020. Knee function through finite
784 element analysis and the role of Miocene hominoids in our understanding of the origin of
785 antipronograde behaviours: the Pierolapithecus catalaunicus patella as a case study.
786 *Palaeontology* 63:459–475. DOI: https://doi.org/10.1111/pala.12466.
787 Pintore R, Houssaye A, Nesbitt SJ, Hutchinson JR. 2021. Femoral specializations to locomotor habits in
788 early archosauriforms. *Journal of Anatomy* 240:867–892. DOI: 10.1111/joa.13598.
789 Polly PD. 2007. Limbs in mammalian evolution. Chapter 15. In: Hall BK ed. *Fins into Limbs: Evolution,*
790 *Development, and Transformation*. Chicago: Brian K. Hall, 245–268.
791 Ponssa ML, Goldberg J, Abdala V. 2010. Sesamoids in Anurans: New Data, Old Issues. *The Anatomical*
792 *Record* 293:1646–1668. DOI: 10.1002/ar.21212.
793 R Core Team. 2014. R: a language and environment for statistical computing.
794 Raux P, Townsend PR, Miegel R, Rose RM, Radin EL. 1975. Trabecular architecture of the human patella.
795 *Journal of Biomechanics* 8:1–7. DOI: 10.1016/0021-9290(75)90037-8.
796 Raymond KR, Prothero DR. 2012. Comparative variability of intermembranous and endochondral bones
797 in Pleistocene mammals. *Palaeontologia Electronica* 13:14.
798 Revell LJ. 2012. phytools: an R package for phylogenetic comparative biology (and other things).
799 *Methods in Ecology and Evolution* 3:217–223. DOI: 10.1111/j.2041-210X.2011.00169.x.
800 Rohlf FJ, Slice D. 1990. Extensions of the Procrustes Method for the Optimal Superimposition of
801 Landmarks. *Systematic Biology* 39:40–59. DOI: 10.2307/2992207.
802 Rubenstein DI. 2011. Family Equidae (Horses and relatives). In: Wilson DE, Mittermeier RA eds.
803 *Handbook of the mammals of the world*. Barcelona: Lynx Edicions, 106–143.

804 Samuels ME, Regnault S, Hutchinson JR. 2017. Evolution of the patellar sesamoid bone in mammals.
805 *PeerJ* 5:e3103. DOI: 10.7717/peerj.3103.
806 Schlager S. 2017. Chapter 9 - Morpho and Rvcg – Shape Analysis in R: R-Packages for Geometric
807 Morphometrics, Shape Analysis and Surface Manipulations. In: Zheng G, Li S, Székely G eds.
808 *Statistical Shape and Deformation Analysis*. Academic Press, 217–256. DOI: 10.1016/B978-0-12-
809 810493-4.00011-0.
810 Schneider MT-Y, Rooks N, Besier T. 2022. Cartilage thickness and bone shape variations as a function of
811 sex, height, body mass, and age in young adult knees. *Scientific Reports* 12:11707. DOI:
812 10.1038/s41598-022-15585-w.
813 Schuurman SO, Kersten W, Weijs WA. 2003. The equine hind limb is actively stabilized during standing.
814 *Journal of Anatomy* 202:355–362. DOI: 10.1046/j.1469-7580.2003.00166.x.
815 Scott KM. 1990. Postcranial dimensions of ungulates as predictors of body mass. In: Damuth JD,
816 MacFadden BJ eds. *Body Size in Mammalian Palaeobiology: Estimation and Biological*
817 *Implications*. Cambridge University Press, 301–335.
818 Seilacher A. 1970. Arbeitskonzept Zur Konstruktions-Morphologie. *Lethaia* 3:393–396. DOI:
819 10.1111/j.1502-3931.1970.tb00830.x.
820 Seilacher A. 1991. Self-Organizing Mechanisms in Morphogenesis and Evolution. In: Schmidt-Kittler N,
821 Vogel K eds. *Constructional Morphology and Evolution*. Berlin, Heidelberg: Springer, 251–271.
822 DOI: 10.1007/978-3-642-76156-0_17.
823 Serio C, Raia P, Meloro C. 2020. Locomotory Adaptations in 3D Humerus Geometry of Xenarthra: Testing
824 for Convergence. *Frontiers in Ecology and Evolution* 8. DOI: 10.3389/fevo.2020.00139.
825 Shockey BJ. 2001. Specialized knee joints in some extinct, endemic, South American herbivores. *Acta*
826 *Palaeontologica Polonica* 46:277–288.

827 Shockey BJ, Mihlbachler MC, Solounias N, Hayes BP. 2008. Functional morphology of the knee in rhinos
828 and the evolution of knee locking mechanisms among rhinocerotoid perissodactyls. *Journal of*
829 *Vertebrate Paleontology* 28:142A.
830 Steiner CC, Ryder OA. 2011. Molecular phylogeny and evolution of the Perissodactyla. *Zoological Journal*
831 *of the Linnean Society* 163:1289–1303. DOI: 10.1111/j.1096-3642.2011.00752.x.
832 Thermo Fisher Scientific. 2018. Avizo.
833 Toumi H, Higashiyama I, Suzuki D, Kumai T, Bydder G, McGonagle D, Emery P, Fairclough J, Benjamin M.
834 2006. Regional variations in human patellar trabecular architecture and the structure of the
835 proximal patellar tendon enthesis. *Journal of Anatomy* 208:47–57. DOI:
836 https://doi.org/10.1111/j.1469-7580.2006.00501.x.
837 Valois H. 1917. La valeur morphologique de la rotule chez les mammifères. *Bulletins et Mémoires de la*
838 *Société d'Anthropologie de Paris* 8:1–34. DOI: 10.3406/bmsap.1917.8819.
839 Vickaryous MK, Olson WM. 2008. Sesamoids and ossicles in the appendicular skeleton. In: Hall BK ed.
840 *Fins into Limbs: Evolution, Development, and Transformation*. Chicago: University of Chicago
841 Press, 323–341.
842 Wasserstein RL, Schirm AL, Lazar NA. 2019. Moving to a World Beyond "p < 0.05." *The American*
843 *Statistician* 73:1–19. DOI: 10.1080/00031305.2019.1583913.
844 Wiley DF, Amenta N, Alcantara DA, Ghosh D, Kil YJ, Delson E, Harcourt-Smith W, Rohlf FJ, St. John K,
845 Hamann B. 2005. Evolutionary Morphing. In: *Proceedings of IEEE Visualization 2005*.
846 Minneapolis, Minnesota,.
847 Zelditch ML, Swiderski DL, Sheets HD, Fink WL. 2012. *Geometric morphometrics for biologists: A Primer*.
848 Academic Press.

849 Zschokke S, Baur B. 2002. Inbreeding, outbreeding, infant growth, and size dimorphism in captive Indian
850 rhinoceros (Rhinoceros unicornis). *Canadian Journal of Zoology* 80:2014–2023. DOI:
851 10.1139/z02-183.

852

853

Figure 1

Main muscular insertions on the patella of a white rhinoceros (*Ceratotherium simum*).

Muscle insertions replaced on the 3D model of *Ceratotherium simum cottoni* AMNH M-51854 based on the anatomical descriptions of Barone 2010a and Etienne et al. 2021.

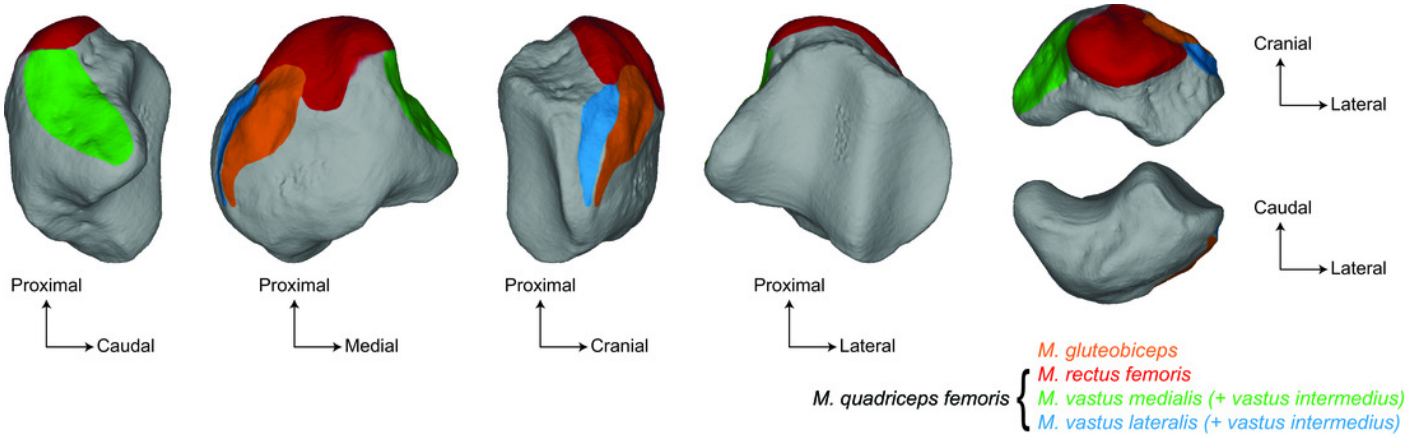

Figure 2

Composite cladogram of the sampled species.

Branch lengths and relations based on Steiner & Ryder, 2011; MacLaren et al., 2018; Bai et al., 2020; Cirilli et al., 2021; Antoine et al., 2021; Liu et al., 2021; Pandolfi et al., 2021. Silhouettes of *C. simum, Dc. bicornis, Ds. sumatrensis, E. z. hartmannae, E. grevyi,* R. sondaicus, *R. unicornis* and *T. indicus* are personal creations. All other silhouettes provided by *www.phylopic.org* under the Creative Commons license.

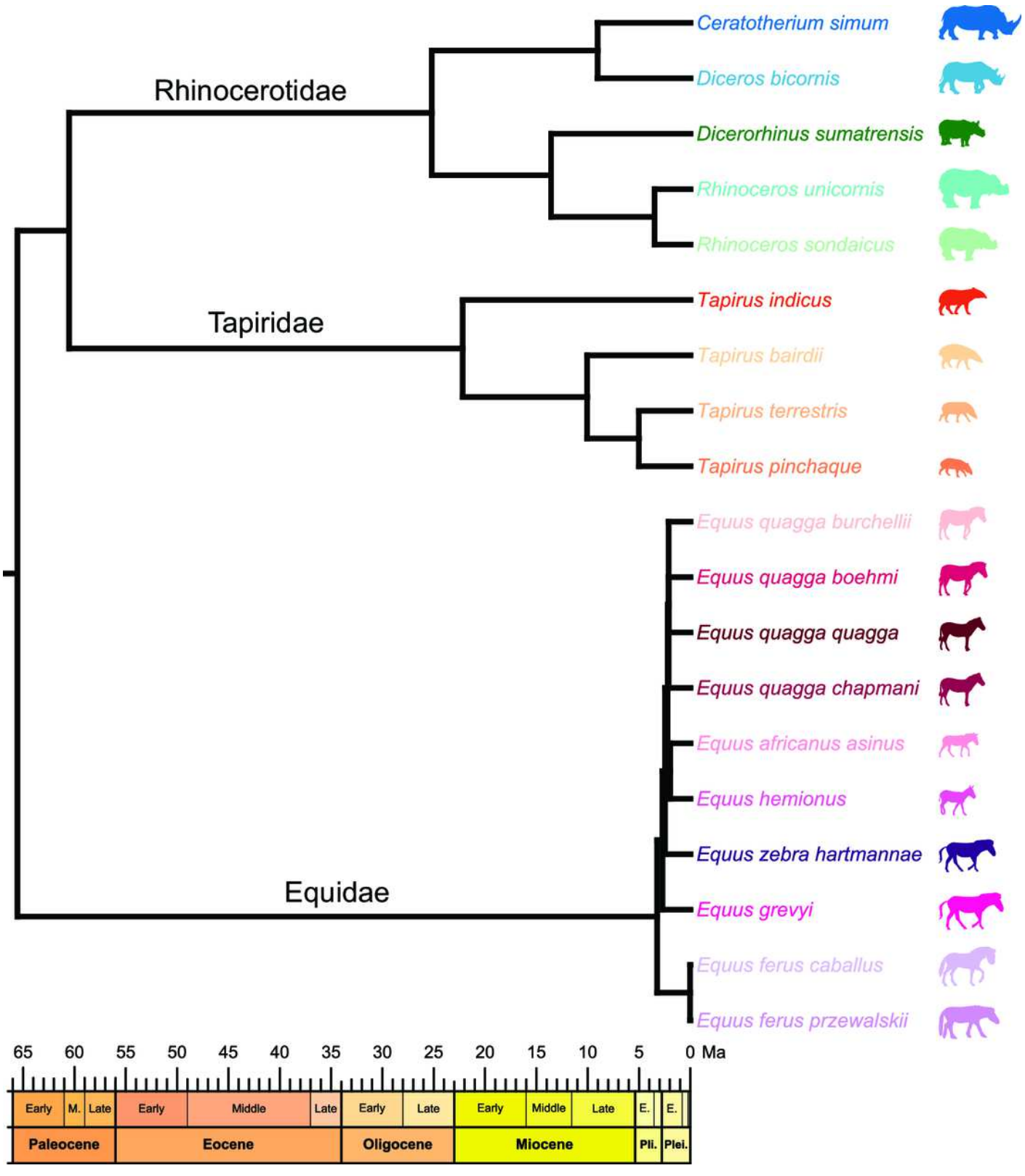
Rhinocerotidae
Tapiridae
Equidae
Ceratotherium simum
Diceros bicornis
Dicerorhinus sumatrensis
Rhinoceros unicornis
Rhinoceros sondaicus
Tapirus indicus
Tapirus bairdii
Tapirus terrestris
Tapirus pinchaque
Equus quagga burchellii
Equus quagga boehmi
Equus quagga quagga
Equus quagga chapmani
Equus africanus asinus
Equus hemionus
Equus zebra hartmannae
Equus grevyi
Equus ferus caballus
Equus ferus przewalskii
65 60 55 50 45 40 35 30 25 20 15 10 5 0 Ma
Early M. Late Early Middle Late Early Late Early Middle Late E. E.
Paleocene Eocene Oligocene Miocene Pli. Plei.

Figure 3

Location of the landmarks used for the analyses.

6 anatomical landmarks (red spheres), 103 curve sliding (blue spheres) and 461 surface sliding (green spheres) semi-landmarks were placed on the patella. Designation of the anatomical landmarks – 1: Most proximal point of the medial ridge; 2: Most distal point of the medial ridge; 3: Most medial point of the medial articular surface; 4: Most proximal point of the medial articular surface; 5: Most proximal point of the base; 6: Most medial point of the medial angle.

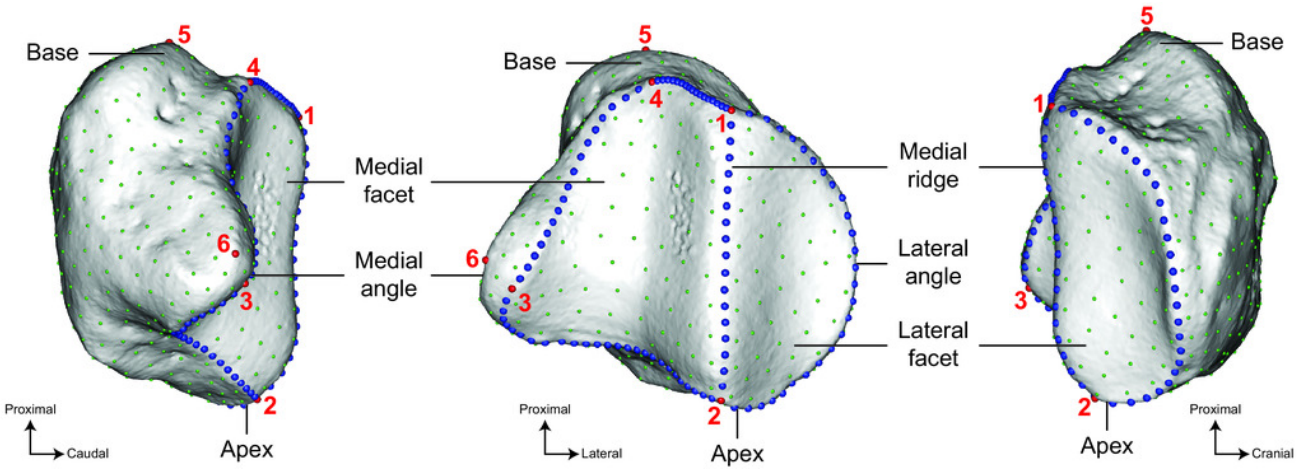

Figure 4

Neighbour Joining tree computed on all PC scores obtained from the PCA performed on shape data of rhinoceroses

Colour code follows Figure 2. Letters indicate sex attribution as in Table 1 (F: female; M: male; U: unknown). Point size is proportional to the mean log centroid size of each specimen. Silhouettes of *C. simum, Dc. bicornis, Ds. sumatrensis, E. z. hartmannae, E. grevyi,* R. sondaicus, *R. unicornis* and *T. indicus* are personal creations. All other silhouettes provided by *www.phylopic.org* under the Creative Commons license. Tree generated by our R code provided as Supplementary Data.

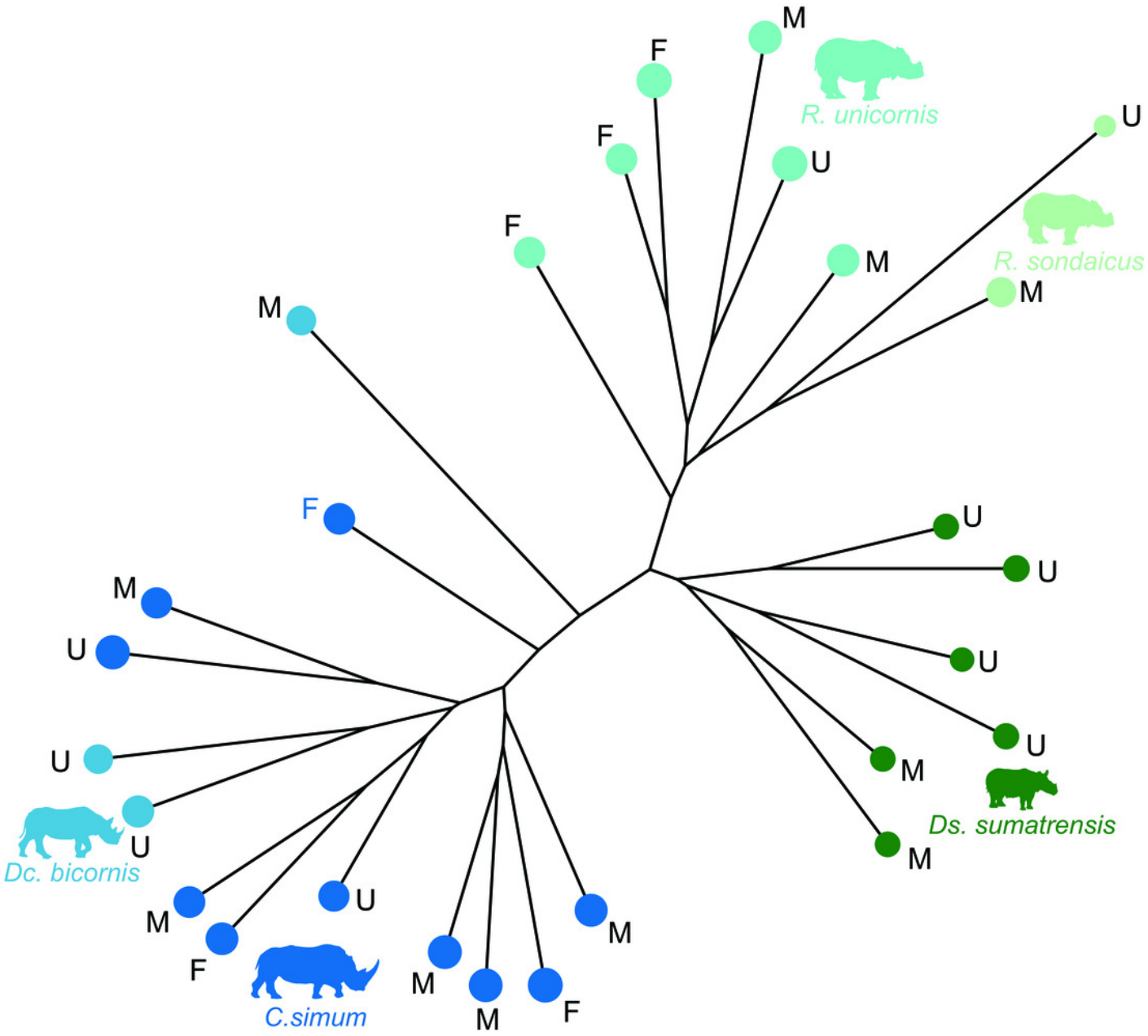
M
F
R. unicornis
F
U
U
F
M
R. sondaicus
M
M
F
U
U
U
M
U
Ds. sumatrensis
M
U
Dc. bicornis
U
M
F
U
C.simum
M
M
M
F

Figure 5

Results of the PCA performed on morphometric data of rhinoceroses and associated shape variation.

A: Morphospace of the two first axes of the PCA with minimal and maximal theoretical shape associated with this variation (respectively in medial and caudal views). Colour codes follow Figure 2. Letters indicate sex attribution as in Table 1. Point size is proportional to the mean log centroid size of each specimen. Silhouettes of *C. simum, Dc. bicornis, Ds. sumatrensis, E. z. hartmannae, E. grevyi,* R. sondaicus, *R. unicornis* and *T. indicus* are personal creations. All other silhouettes provided by *www.phylopic.org* under the Creative Commons license. **B**: Morphological variation between minimal (light brown) and maximal (light grey) theoretical shapes along a) PC1 and b) PC2 respectively in medial, cranial, lateral, caudal, dorsal (top) and ventral (bottom) views. Intensities of landmark displacements are shown with vector colorations ranging from blue (low distance) to red (high distance). Plot and theoretical 3D models generated by our R code provided as Supplementary Data (using the specimen *Dicerorhinus sumatrensis* AMNH M-81892 as a template for deformation of the meshes).

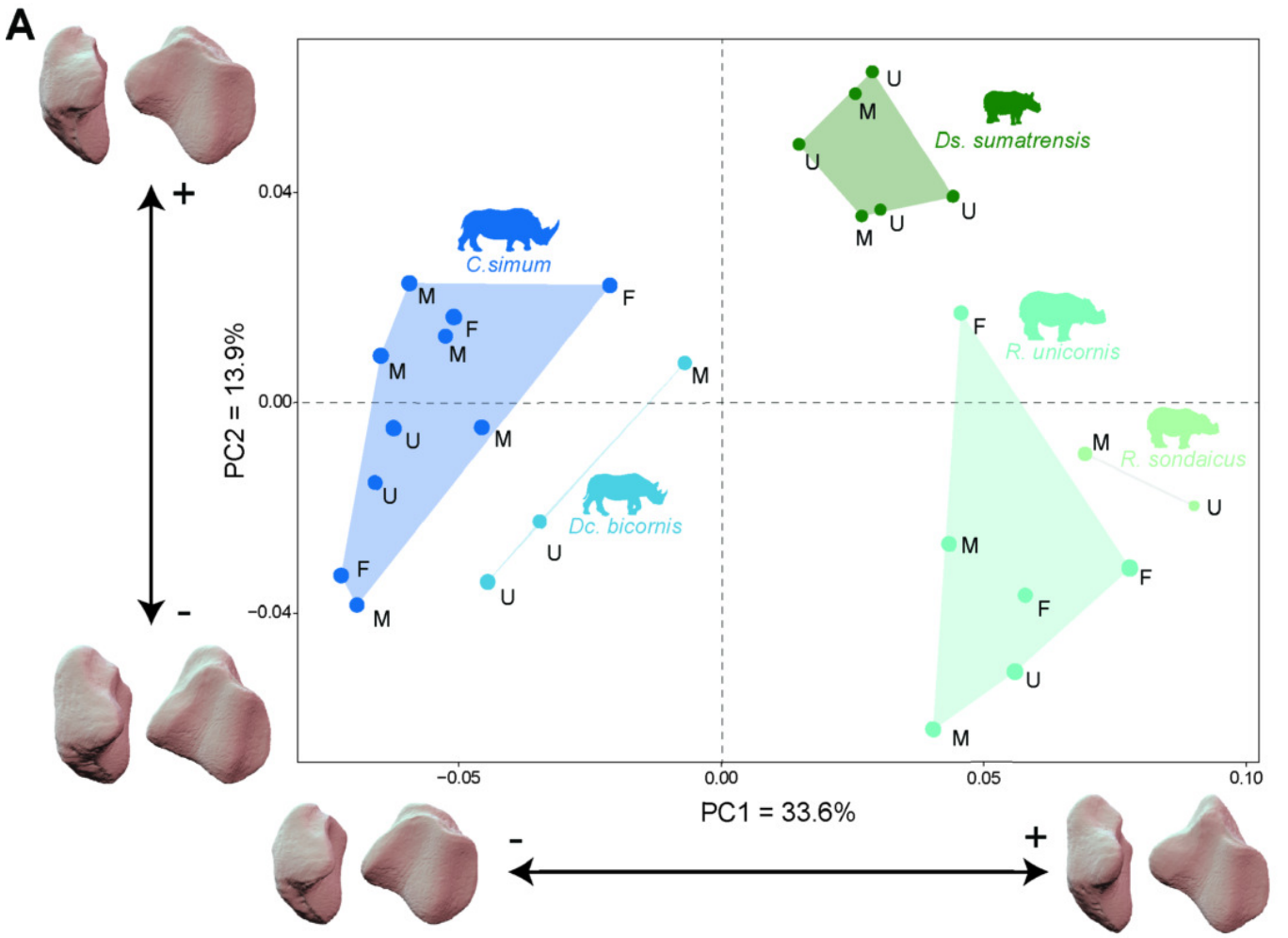
A
+
-
0.04
0.00
−0.04
PC2 = 13.9%
C.simum
Ds. sumatrensis
Dc. bicornis
R. unicornis
R. sondaicus
M
F
U
−0.05
0.00
0.05
0.10
PC1 = 33.6%
-
+

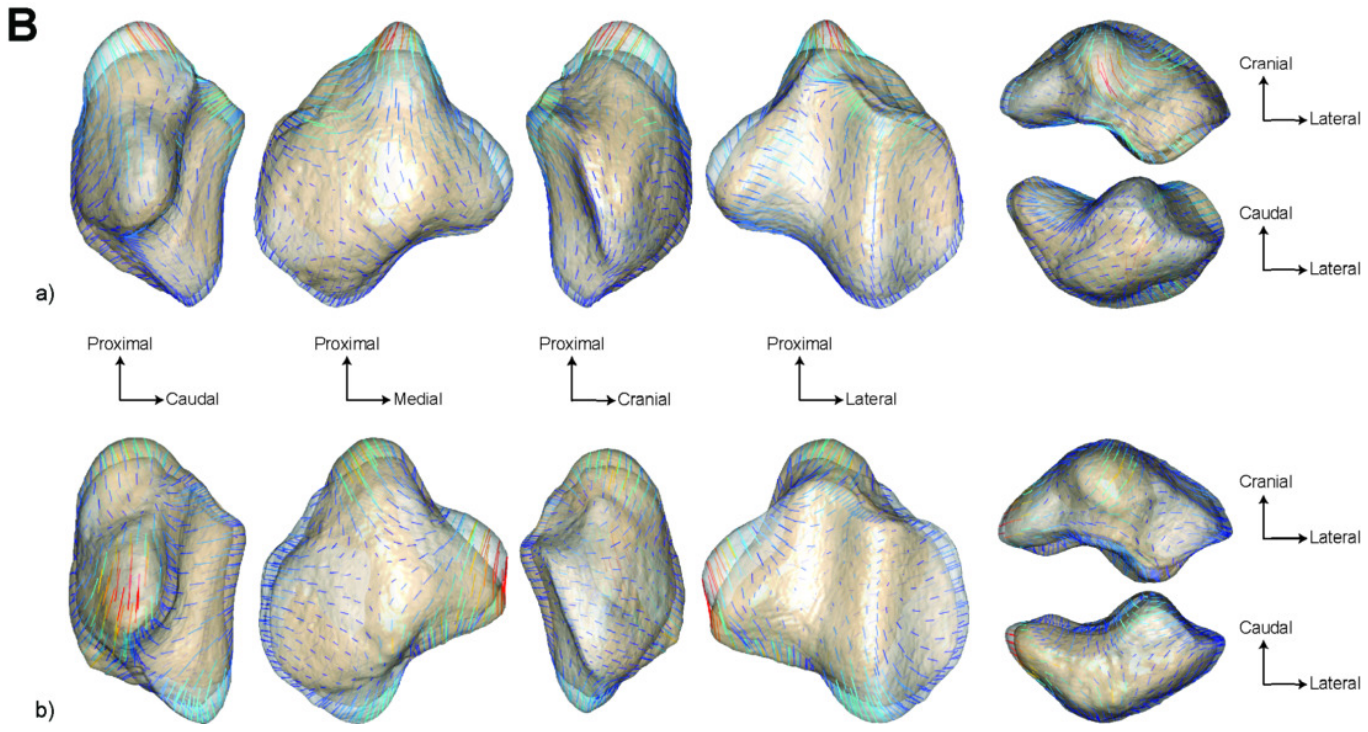
B
a)
b)
Proximal
Caudal
Proximal
Medial
Proximal
Cranial
Proximal
Lateral
Cranial
Lateral
Caudal
Lateral

Figure 6

Results of the Procrustes ANOVA on shape data against log-transformed centroid size (CS) for rhinos

A: Regression plot with theoretical shapes associated with minimum and maximum fitted values (respectively in medial and caudal views). Colour code follows Figure 2. Point size is proportional to the mean log centroid size of each specimen. Symbols indicate the sex attribution (triangle: male; circle: female; square: unknown). Silhouettes of *C. simum, Dc. bicornis, Ds. sumatrensis, E. z. hartmannae, E. grevyi,* R. sondaicus, *R. unicornis* and *T. indicus* are personal creations. All other silhouettes provided by *www.phylopic.org* under the Creative Commons license. **B:** Colour maps of the location and intensity of the shape deformation. The shape associated with the maximal CS value of the Procrustes ANOVA was coloured depending on its distance to the shape associated with the minimal value. Green indicates no deformation; blue indicates a negative deformation of high intensity; red indicates a positive deformation of high intensity. Plot and theoretical 3D models generated by our R code provided as Supplementary Data. Plot and theoretical 3D models generated by our R code provided as Supplementary Data (using the specimen *Dicerorhinus sumatrensis* AMNH M-81892 as a template for deformation of the meshes).

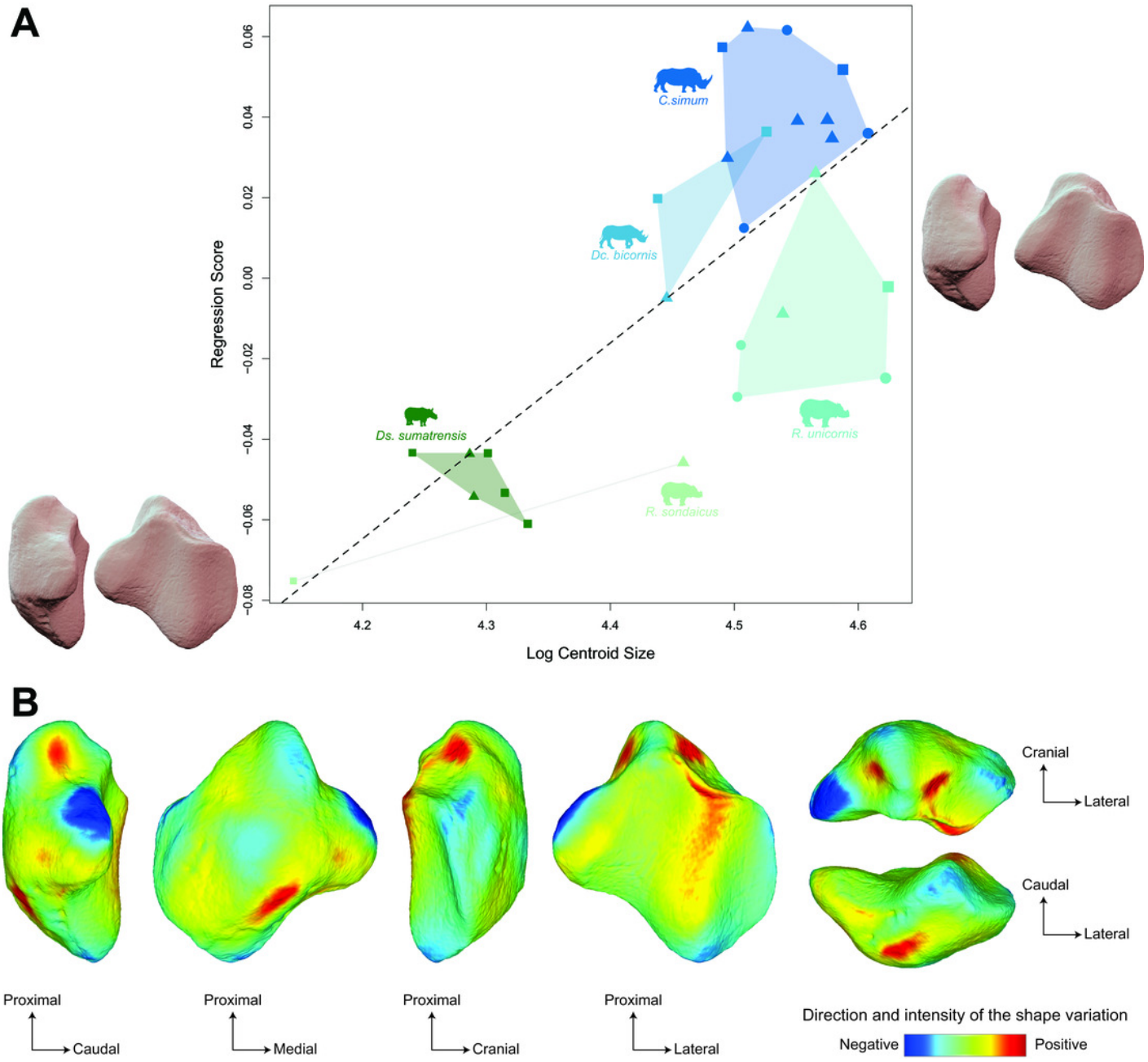
A
Regression Score
0.06
0.04
0.02
0.00
−0.02
−0.04
−0.06
−0.08
4.2
4.3
4.4
4.5
4.6
Log Centroid Size
C.simum
Dc. bicornis
Ds. sumatrensis
R. unicornis
R. sondaicus
B
Proximal
Caudal
Proximal
Medial
Proximal
Cranial
Proximal
Lateral
Cranial
Lateral
Caudal
Lateral
Direction and intensity of the shape variation
Negative
Positive

Figure 7

Neighbour Joining tree computed on all PC scores obtained from the PCA performed on shape data of all perissodactyls.

Colour code follows Figure 2. Symbols indicate age class as in Table 1 (triangle: subadult; circle: adult). Point size is proportional to the mean log centroid size of each specimen. Silhouettes of *C. simum, Dc. bicornis, Ds. sumatrensis, E. z. hartmannae, E. grevyi,* R. sondaicus, *R. unicornis* and *T. indicus* are personal creations. All other silhouettes provided by *www.phylopic.org* under the Creative Commons license. Tree generated by our R code provided as Supplementary Data.

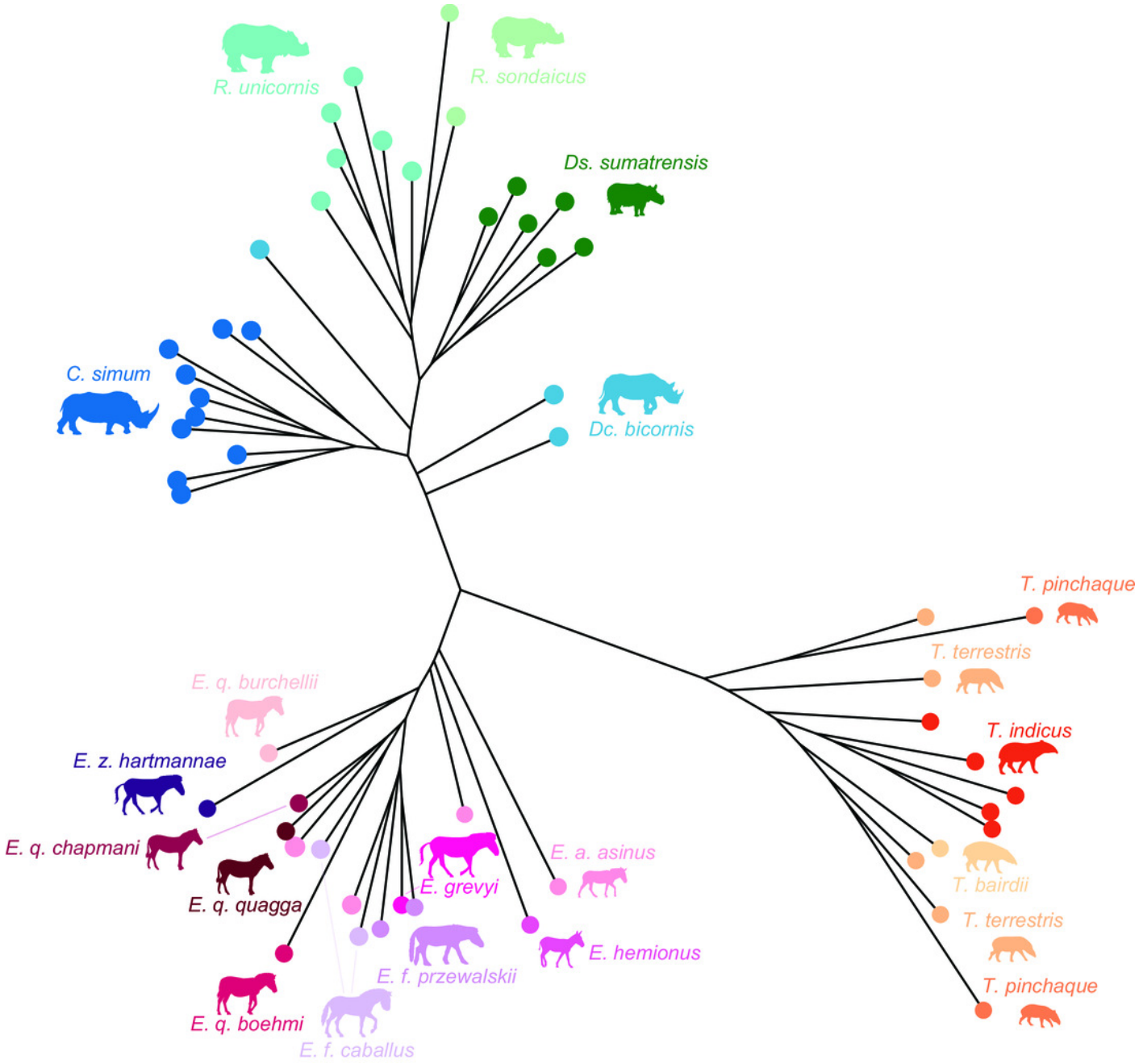
R. unicornis
R. sondaicus
Ds. sumatrensis
C. simum
Dc. bicornis
T. pinchaque
T. terrestris
T. indicus
T. bairdii
T. terrestris
T. pinchaque
E. q. burchellii
E. z. hartmannae
E. q. chapmani
E. q. quagga
E. q. boehmi
E. f. caballus
E. f. przewalskii
E. grevyi
E. a. asinus
E. hemionus

Figure 8

Results of the PCA performed on morphometric data of all perissodactyls and associated shape variation.

A: Morphospace of the two first axes of the PCA with minimal and maximal theoretical shape associated with this variation (respectively in medial and caudal views). Colour codes follow Figure 2. Point size is proportional to the mean log centroid size of each specimen. Silhouettes of *C. simum, Dc. bicornis, Ds. sumatrensis, E. z. hartmannae, E. grevyi,* R. sondaicus, *R. unicornis* and *T. indicus* are personal creations. All other silhouettes provided by *www.phylopic.org* under the Creative Commons license. **B**: Morphological variation between minimal (light brown) and maximal (light grey) theoretical shapes along a) PC1 and b) PC2 respectively in medial, cranial, lateral, caudal, dorsal (top) and ventral (bottom) views. Intensities of landmark displacements are shown with vector colorations ranging from blue (low distance) to red (high distance). Plot and theoretical 3D models generated by our R code provided as Supplementary Data (using the specimen *Diceros bicornis* NHMUK ZD 1879.9.26.6 as a template for deformation of the meshes).

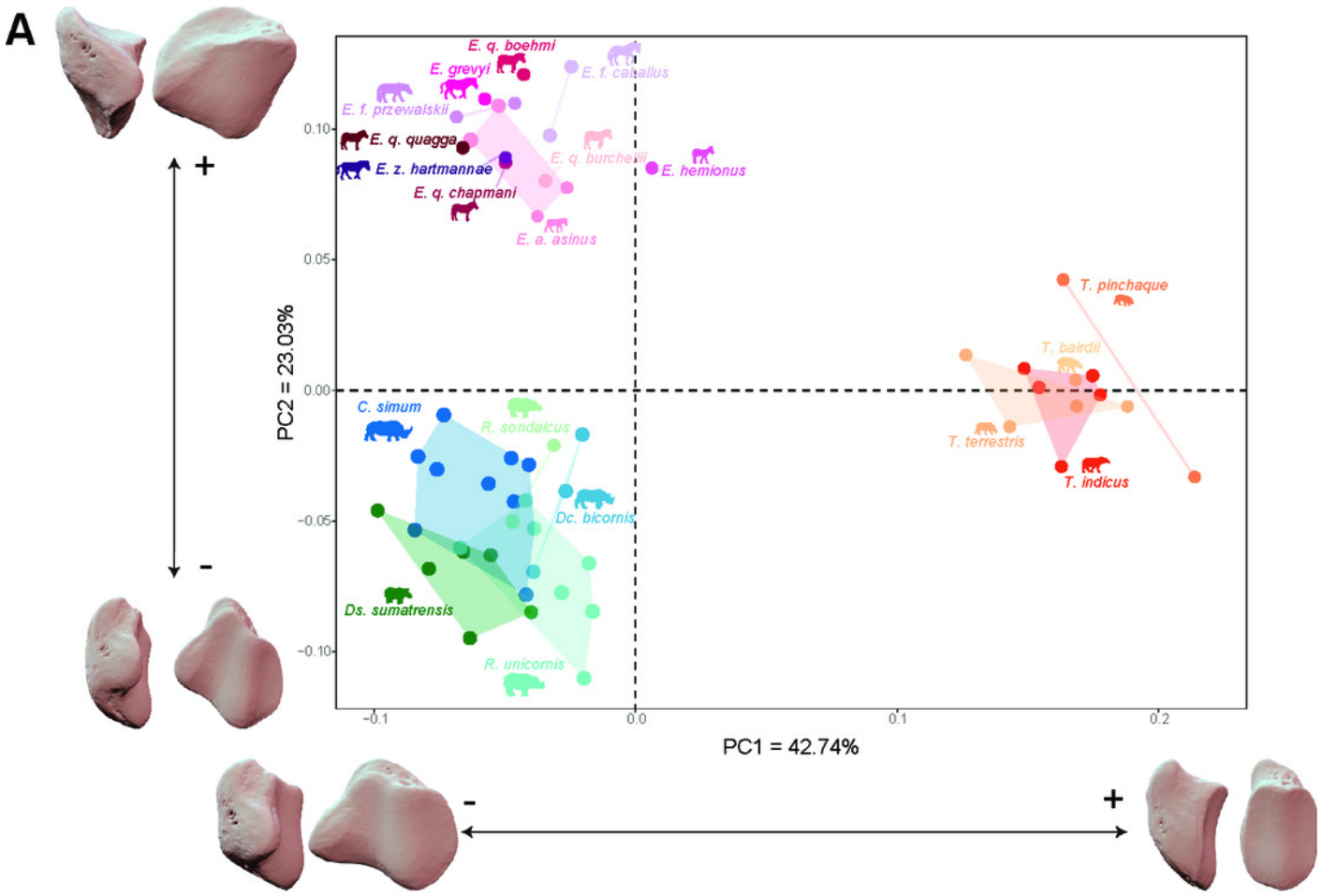
A
E. q. boehmi
E. grevyi
E. f. caballus
E. f. przewalskii
E. q. quagga
E. z. hartmannae
E. q. chapmani
E. q. burchelli
E. hemionus
E. a. asinus
T. pinchaque
T. bairdii
T. terrestris
T. indicus
C. simum
R. sondaicus
Dc. bicornis
Ds. sumatrensis
R. unicornis
PC2 = 23.03%
PC1 = 42.74%
0.10
0.05
0.00
−0.05
−0.10
−0.1
0.0
0.1
0.2
+
-
+
-

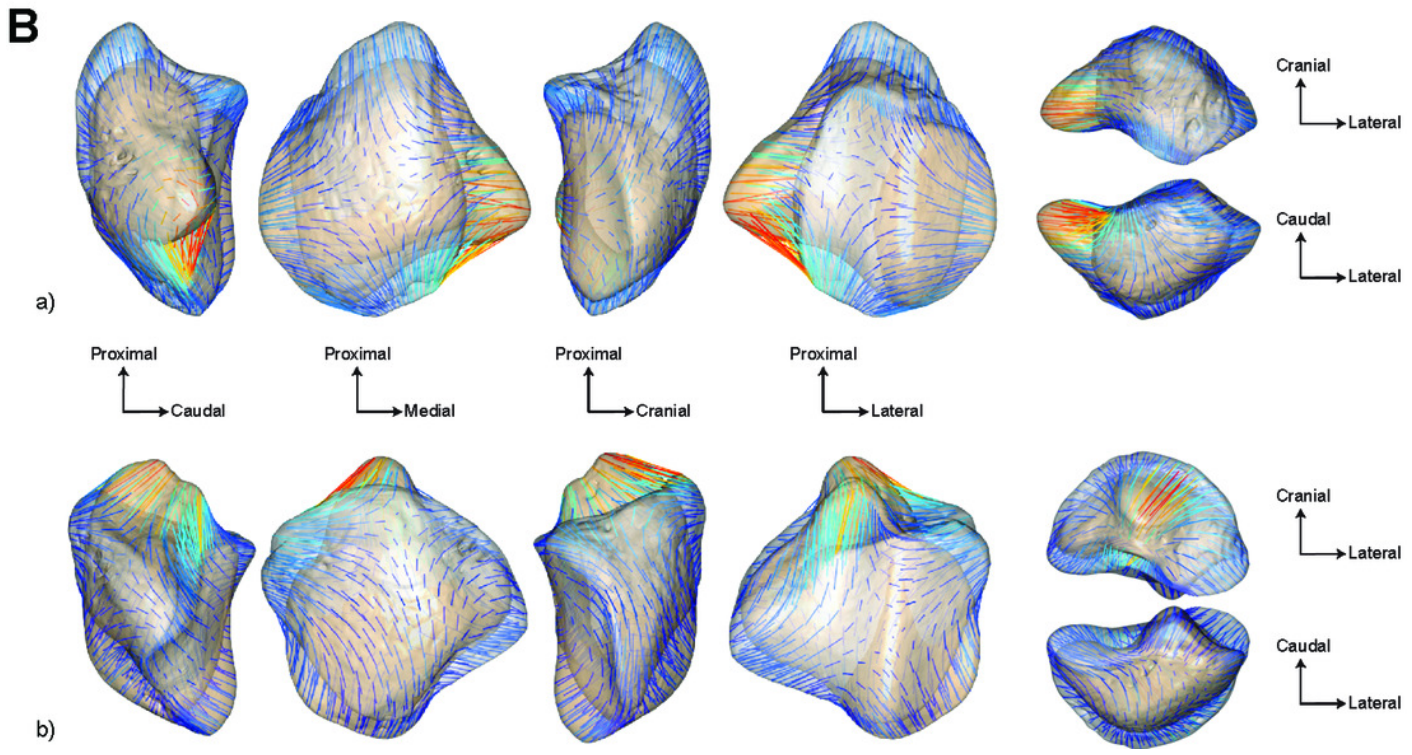
B
a)
b)
Proximal
Caudal
Proximal
Medial
Proximal
Cranial
Proximal
Lateral
Cranial
Lateral
Caudal
Lateral
Cranial
Lateral
Caudal
Lateral

Figure 9

Results of the Procrustes ANOVA on shape data against log-transformed centroid size (CS) for all perissodactyls.

A: Regression plot with theoretical shapes associated with minimum and maximum fitted values (respectively in medial and caudal views). Colour code follows Figure 2. Point size is proportional to the mean log centroid size of each specimen. Silhouettes of *C. simum, Dc. bicornis, Ds. sumatrensis, E. z. hartmannae, E. grevyi,* R. sondaicus, *R. unicornis* and *T. indicus* are personal creations. All other silhouettes provided by *www.phylopic.org* under the Creative Commons license. **B:** Colour maps of the location and intensity of the shape deformation. The shape associated with the minimal CS value of the Procrustes ANOVA was coloured depending on its distance to the shape associated with the maximal value. Green indicates no deformation; blue indicates a negative deformation of high intensity; red indicates a positive deformation of high intensity. Plot and theoretical 3D models generated by our R code provided as Supplementary Data (using the specimen *Diceros bicornis* NHMUK ZD 1879.9.26.6 as a template for deformation of the meshes).

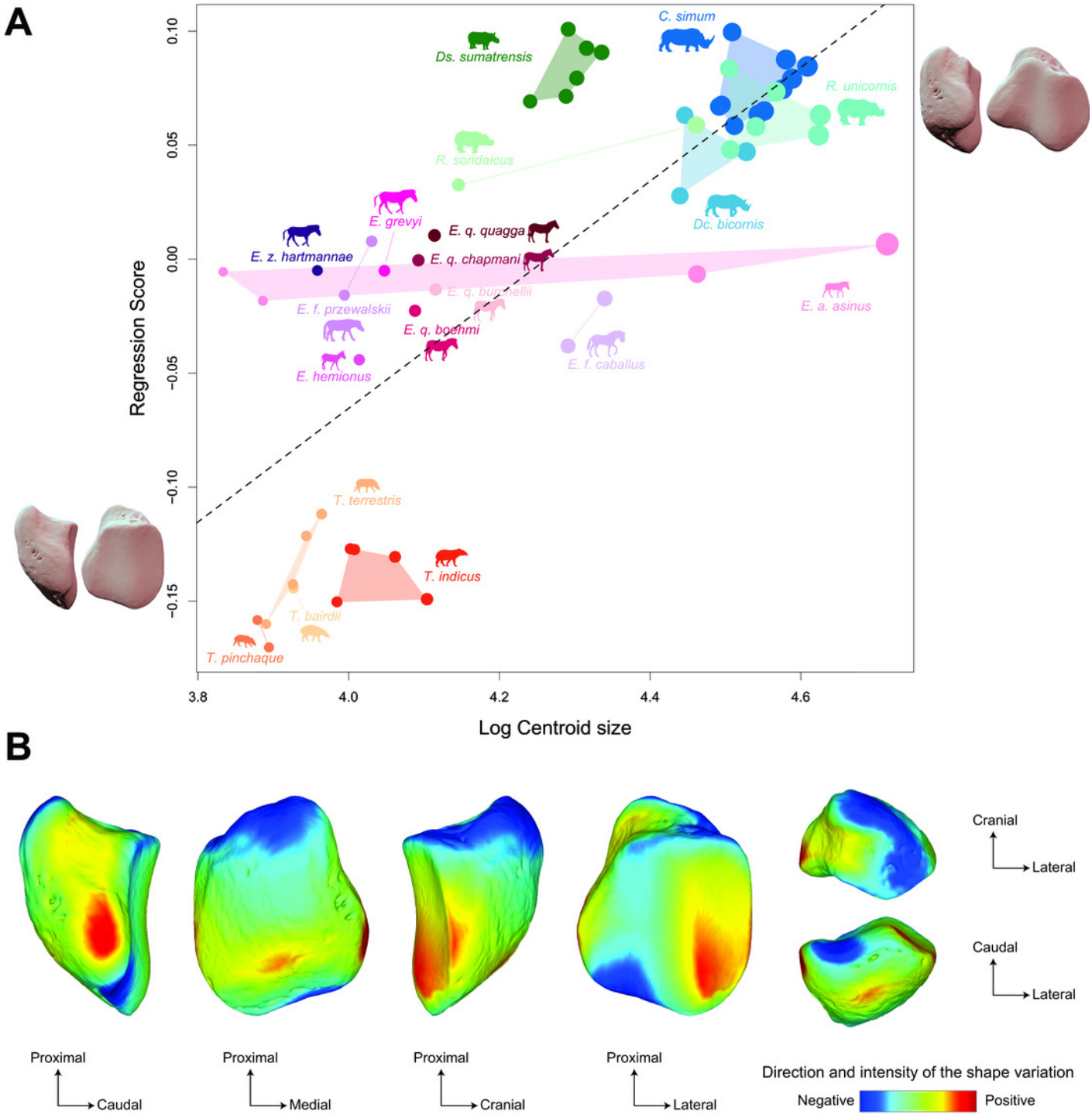
A
C. simum
Ds. sumatrensis
R. unicornis
R. sondaicus
Dc. bicornis
E. grevyi
E. q. quagga
E. z. hartmannae
E. q. chapmani
E. q. burchelli
E. f. przewalskii
E. a. asinus
E. q. boehmi
E. f. caballus
E. hemionus
T. terrestris
T. indicus
T. bairdii
T. pinchaque
Regression Score
0.10
0.05
0.00
−0.05
−0.10
−0.15
3.8
4.0
4.2
4.4
4.6
Log Centroid size
B
Proximal
Caudal
Proximal
Medial
Proximal
Cranial
Proximal
Lateral
Cranial
Lateral
Caudal
Lateral
Direction and intensity of the shape variation
Negative
Positive

Table 1(on next page)

List of the studied specimens with family, genus and species names, mean body mass, institutions, sex, age class, condition, and 3D acquisition details.

Abbreviations: Sex: F: female; M: male; U: unknown. Age – A: adult; S: sub-adult. Condition – W: wild; C: captive; U: unknown. 3D acquisition – LS: laser scanner; SL: structured light surface scanner; P: photogrammetry; CT: CTscan. Stars indicate specimens retrieved on MorphoSource deposit. Institutional codes – AMNH: American Museum of Natural History. BICPC: Powell Cotton Museum, Birchington-on-Sea. IMNH: Idaho Museum of Natural History, Pocatello. MNHN: Muséum National d'Histoire Naturelle, Paris. MVZ: Museum of Vertebrate Zoology, Berkeley. NHMUK: Natural History Museum, London. NMB: Naturhistorisches Museum Basel, Basel. RBINS: Royal Belgian Institute of Natural Sciences, Brussels.

Family	Taxon	Mean body maSL (kg)	Institution	Collection number	Sex	Age	Condition	3D acquisition
Rhinocerotidae	*Ceratotherium simum*	2,300	AMNH	M-51854	F	A	W	SL
			AMNH	M-51855	M	A	W	SL
			AMNH	M-51857	F	A	W	SL
			AMNH	M-51858	M	A	W	SL
			AMNH	M-81815	U	A	U	SL
			BICPC	NH.CON.37	F	A	W	SL
			BICPC	NH.CON.110	M	A	W	SL
			BICPC	NH.CON.112	M	A	W	SL
			MNHN	ZM-MO-2005-297	M	A	C	CT
			NHMUK	ZD 2018.143	U	A	U	SL
	Diceros bicornis	1,050	AMNH	M-113777	U	A	W	SL
			MNHN	ZM-AC-1944-278	M	A	C	CT
			NHMUK	ZD 1879.9.26.6	U	U	U	CT
	Dicerorhinus sumatrensis	775	AMNH	M-81892	M	A	W	SL
			NHMUK	ZD 1879.6.14.2	M	A	W	SL
			NHMUK	ZD 1894.9.24.1	U	A	W	SL
			NHMUK	ZE 1948.12.20.1	U	A	U	SL
			NHMUK	ZE 1949.1.11.1	U	A	W	SL
			NHMUK	ZD 2004.23	U	A	W	SL
	Rhinoceros sondaicus	1,350	MNHN	ZM-AC-A7970	U	A	U	SL
			NHMUK	ZD 1871.12.29.7	M	A	W	SL
	Rhinoceros unicornis	2,000	AMNH	M-35759	M	A	C	SL
			AMNH	M-54454	F	A	W	SL
			MNHN	ZM-AC-1967-101	F	A	C	SL
			NHMUK	ZE 1961.5.10.1	M	A	W	SL
			NHMUK	ZD 1972.822	U	A	U	SL
			NHMUK	ZD 1884.12.1.2	F	A	W	SL
Tapiridae	*Tapirus bairdii*	260	MVZ	141172	U	A	U	LS*
	Tapirus indicus	340	MNHN	ZM-AC-1931-528	M	A	C	CT
			MNHN	ZM-AC-1945-460	M	A	C	CT
			NMB	8125	F	A	C	CT
			RBINS	1184D	M	A	C	LS
			RBINS	1184E	M	A	C	LS
	Tapirus pinchaque	175	MNHN	ZM-AC-1982-34	M	A	C	CT
			MNHN	Indet	U	A	U	CT
	Tapirus terrestris	220	MNHN	ZM-AC-1937-1	U	A	C	CT
			MNHN	ZM-MO-1990-20	M	A	C	CT
			RBINS	1185D	M	A	C	LS
			RBINS	1185E	U	A	C	LS
Equidae	*Equus africanus asinus*	275	MNHN	ZM-AC-1893-634	M	A	C	CT

		MNHN	ZM-2005-717	U	A	U	CT
		RBINS	12970	F	A	C	LS
		RBINS	13076	F	A	C	LS
Equus hemionus	230	MNHN	ZM-AC-1880-1103	M	A	C	CT
Equus ferus caballus	490	MNHN	ZM-AC-A541	F	A	C	CT
		MVZ	162289	M	A	C	LS*
Equus ferus przewalskii	250	MNHN	ZM-AC-1975-124	F	A	C	CT
		RBINS	14281	M	A	C	LS
Equus burchellii granti	247	RBINS	33386	U	A	U	LS
Equus grevyi	400	RBINS	32166	M	A	C	LS
Equus quagga boehmi	247	RBINS	12129	M	A	W	LS
Equus quagga chapmani	247	RBINS	1218	F	A	C	LS
Equus quagga quagga	247	IMNH	R2425	U	A	U	LS*
Equus zebra hartmannae	310	RBINS	3974	M	S	C	LS

1

Table 2(on next page)

Results of the Pearson's correlation tests between the log-transformed centroid size and the two first principal components of the PCA, for rhinoceroses only and all perissodactyls respectively.

Abbreviations: r, Pearson's correlation coefficient value; t, Student distribution value; dF, degrees of freedom; P, p value. Significant results are indicated in bold.

	Component	r	t	dF	P
Rhinoceroses	**PC1**	**-0.41**	**-2.24**	**25**	**0.03**
	PC2	**-0.55**	**-3.278**	**25**	**<0.01**
All perissodactyls	**PC1**	**-0.61**	**-5.60**	**52**	**<0.01**
	PC2	**-0.48**	**-3.96**	**52**	**<0.01**

1

Table 3(on next page)

Results of the PERMANOVAs performed on PC scores against specific attribution and sex, for rhinoceroses only and all perissodactyls respectively.

Abbreviations: dF, degrees of freedom; R^2: coefficient of partial determination; F: F-statistics; P, p value. Significant results are indicated in bold.

		Df	Sum of Squares	R^2	F	P
Rhinoceroses	Species	**4**	**0.08**	**0.59**	**4.20**	**<0.01**
	Sex	1	<0.01	0.03	0.90	0.47
	Residuals	11	0.05	0.38		
	Total	16	0.13	1		
All perissodactyls	Species	**15**	**0.62**	**0.86**	**8.34**	**<0.01**
	Sex	1	<0.01	<0.01	0.74	0.563
	Residuals	20	0.10	0.14		
	Total	36	0.72	1		

1

Table 4(on next page)

Results of the Procrustes ANOVAs on shape data against log centroid size and femoral circumference respectively, for rhinoceroses only and all perissodactyls respectively.

Abbreviations: dF: degrees of freedom; R^2: coefficient of determination; F: F-statistics; Z: Z score; P: p value. Significant results are indicated in bold.

		dF	Sum of Squares	R^2	F	Z	P
Rhinoceroses only	Log Centroid size	1	**0.03**	**0.12**	**3.37**	**2.57**	**<0.001**
	Residuals	25	0.19	0.88			
	Total	26	0.22				
	Log Femoral circumference	**1**	**0.02**	**0.12**	**3.20**	**2.33**	**0.01**
	Residuals	24	0.18	0.88			
	Total	25	0.21				
All perissodactyls	Log Centroid size	1	**0.23**	**0.22**	**14.74**	**4.13**	**<0.01**
	Residuals	52	0.81	0.78			
	Total	53	1.04				
	Log Femoral circumference	1	**0.25**	**0.26**	**17.27**	**4.40**	**<0.01**
	Residuals	50	0.73	0.74			
	Total	51	0.99				

1